

Article

Scallion Peel Mediated Synthesis of Zinc Oxide Nanoparticles and Their Applications as Nano fertilizer and Photocatalyst for Removal of Organic Pollutants from Wastewater

Soufiane Soltani ¹, Amel Gacem ² , Nisha Choudhary ³, Virendra Kumar Yadav ^{4,*} , Huda Alsaedi ⁵ , Shreya Modi ⁶, Aradhana Patel ⁷, Samreen Heena Khan ⁸ , Marina M. S. Cabral-Pinto ⁹ , Krishna Kumar Yadav ^{10,*}  and Ashish Patel ^{3,*}

- ¹ Department of Physics, Physical Chemistry of Surfaces and Interfaces Research Laboratory of Skikda (LRPCSI), University of Skikda, Skikda 21000, Algeria
 - ² Department of Physics, Faculty of Sciences, University 20 Aout 1955, Skikda 21000, Algeria
 - ³ Department of Life Sciences, Hemchandracharya North Gujarat University, Patan 384265, India
 - ⁴ Department of Biosciences, School of Liberal Arts & Sciences, Mody University of Science and Technology, Lakshmangarh, Sikar 332311, India
 - ⁵ Department of Chemistry, College of Science, King Saud University, Riyadh 11451, Saudi Arabia
 - ⁶ Department of Microbiology, Shri Sarvajanic Science College, Hemchandracharya North Gujarat University, Mehsana 384001, India
 - ⁷ Department of Microbiology, Faculty of Sciences, Sankalchand Patel University, Mehsana 384315, India
 - ⁸ Department of Research and Development, YNC Envis Private Limited, New Delhi 110059, India
 - ⁹ Geobiotec Research Centre, Department of Geoscience, University of Aveiro, 3810-193 Aveiro, Portugal
 - ¹⁰ Faculty of Science and Technology, Madhyanchal Professional University, Bhopal 462044, India
- * Correspondence: yadava94@gmail.com (V.K.Y.); envirokrishna@gmail.com (K.K.Y.); uni.ashish@gmail.com (A.P.)



Citation: Soltani, S.; Gacem, A.; Choudhary, N.; Yadav, V.K.; Alsaedi, H.; Modi, S.; Patel, A.; Khan, S.H.; Cabral-Pinto, M.M.S.; Yadav, K.K.; et al. Scallion Peel Mediated Synthesis of Zinc Oxide Nanoparticles and Their Applications as Nano fertilizer and Photocatalyst for Removal of Organic Pollutants from Wastewater. *Water* **2023**, *15*, 1672. <https://doi.org/10.3390/w15091672>

Academic Editors: Chengyun Zhou, Zakaria Al-Qodah and Khalid Bani-Melhem

Received: 18 February 2023
Revised: 22 March 2023
Accepted: 27 March 2023
Published: 25 April 2023



Copyright: © 2023 by the authors. Licensee MDPI, Basel, Switzerland. This article is an open access article distributed under the terms and conditions of the Creative Commons Attribution (CC BY) license (<https://creativecommons.org/licenses/by/4.0/>).

Abstract: Nanotechnology and nanomaterials have gained much attention in recent years due to their remarkable features. Among nanoparticles, photocatalytic material, such as zinc oxide, have shown tremendous applications in each and every field of science. In the present research, investigators have synthesized zinc oxide nanoparticles (ZnONPs) using Scallion's peel extract. ZnONPs were both spherical and rod-shaped, where the size for spherical particles was 40–100 nm and rod-shaped, particles size was more than 200 nm as confirmed by microscopic techniques. The typical trademark bands of ZnONPs at 400–800 cm⁻¹ were revealed by infrared spectroscopy, which also showed bands of carbonyl and hydroxyl groups. The hydrodynamic size by particle size analyzer (PSA) shows a size near about 200 nm in diameter. Furthermore, the synthesized ZnONPs were used to assess their potential as a micronutrient for the plant and nano adsorbent for the removal of antibiotics (ampicillin) and methylene blue dye from the simulated wastewater. The antibiotic and dye removal were observed under UV light and visible light against contact time. In comparison to control seeds, seeds grown with ZnONPs have shown better germination and seedling. It could be concluded that ZnONPs acted as an important nanosized source of nutrition for agricultural applications. Thus, the effect of ZnONPs has been proven as a nano-based nutrient source for agricultural purposes. The remediation study found that remediation of both ampicillin and methylene blue dye was efficient under UV light under similar experimental parameters from the simulated wastewater by the ZnONPs.

Keywords: wastewater; spring onion; simulated wastewater; photocatalytic; antibiotics

1. Introduction

Nanotechnology deals with producing and using materials up to 100 nm in size [1]. The novel properties of nanoparticles (NPs) are extensively applied in various fields for instance material science, food industry, cosmeceuticals, medicines, biomedical devices,

environmental remediation, agriculture, packaging, and information technology applications [2]. Among different types of NPs, metal oxide NPs are considered more valuable because of their unique properties. Zinc oxide nanoparticles (ZnO-NPs) have been attracting the attention of investigators in couple last few years due to their photocatalytic nature, high surface area to volume ratio (SVR), and high efficiency [3]. Zinc and its oxide forms have several important roles in a biological system, for instance, synthesis and degradation of carbohydrates, proteins, lipids, and nucleic acids [4]. Zn deficiency causes several abnormalities in plants, such as chlorosis, small leaves, and stunted growth. It is required for auxin synthesis and actively activates enzymes, such as phosphoryl hydrolase, dehydrogenase, protease, and peptide [5].

The various pieces of the literature show that the soil properties hamper the efficient nutrient uptake from the soil, especially NPs. Thus, there is a need for a biologically mediated synthesis of ZnONPs, which should also be economical. In addition to this, if the biological synthesis is from waste material, then the cost of NPs and ultimately its application technique cost will also be lower [6].

Scallions (spring onion) peel is rich in several phytochemicals, which may help in the formation of ZnONPs of desired morphology. Previously, several investigators reported the phyto-mediated ZnONPs, for instance Demissie et al. (2020) synthesized ZnONPs by using extracts of Koseret leaves (*Lippia adoensis*), where the size of NPs was 22 nm (average size). The investigators have further assessed the Koseret leaves-mediated synthesized ZnONPs' potential for antibacterial activity against Gram-positive and Gram-negative bacteria [7]. Naseer (2020) synthesized ZnONPs using *Cassia fistula* and *Melia azadarach* via green synthesis and studied their antimicrobial activities [8]. Kahsay (2021) reported the synthesis of ZnONPs whose average crystallite size was found to be 20 nm as calculated by XRD. ZnONPs were synthesized by using *Becium grandiflorum* aqueous leaf extract which was further applied as an antimicrobial agent and adsorption of methylene blue Faisal and their team reported the synthesis of ZnONPs from the aqueous extract of the fruit of *Myristica fragrans*. Moreover, investigators further utilized the synthesized ZnONPs for biomedical and environmental applications [9]. In another approach, a team led by Alamdari used *Sambucus ebulus* leaves extract for the synthesis of the wurtzite phase of ZnONPs with an average size of 17 nm [10]. Modi and Fulekar, (2020) used peel extracts of *Allium sativum* for the synthesis of ZnONPs. In addition to this, there are several examples where investigators observed the effect of ZnONPs on crop and non-crop plant growth. Recently, Modi and their team synthesized ZnONPs from the dried peel of onion (from the vegetable market) and showed its toxicity on the growth of the *Triticum sativaum* plant [11]. One more recent attempt made by a team led by Iqbal synthesized ZnONPs of an average size of about (26 nm) by using *Elaeagnus angustifolia* (EA) leaf extracts [12]. Fakhari and their colleagues used the leaf extracts of *Laurus nobilis* L. for the preparation of ZnONPs by using various precursors of zinc [13].

Nanotechnology has shown drastic developments in the agricultural sectors in recent years. It is widely used in agriculture sectors as nano fertilizers, nano agrochemicals, nanosensors, nano pesticides, and nano herbicides [14]. All these help in the increase in food production, and ensure sustainable agriculture and food security. Being nano-sized, all these agriculturally important materials have a high surface area to volume ratio (SVR), which have numerous advantages, such as more adsorption sites, and more surface area for interaction with minerals, nutrients, or with plant roots. Several investigators have shown the use of nanomaterials and nanofibers in the agriculture sector for instance Mamun and their teams have provided a depth investigation of the NPs in the agriculture sector. Investigators emphasized the importance of nano fertilizers, due to high SVR, and slow release of nutrients to the plants [4].

Previously several investigators have also tried to synthesize ZnONPs biologically, for instance, Li and their team synthesized ZnO microtubes by using hemp fibers as a temple. The size of the agglomerated ZnO microtubes was up to 100 nm with lattice fringes of 0.248 nm. The particle was crystalline and confirmed by the XRD and scattering

area electron diffraction pattern (SAED). Finally, the synthesized ZnO microtubes were used for the low temperature, nitric oxide gas sensing at ppb level [15]. Mansour and their team reported the synthesis of ZnONPs using red seaweed whose surface area was $113.751 \text{ m}^2 \text{ g}^{-1}$ and an average pore size of 2.527 nm. The ZnONPs were used for the removal of IVR2 dye, and removal was about 99% at 6 pH [16]. Song and their team also synthesized porous ZnO microtubules for the selective detection of nitric oxide at ppb level at low temperature [17].

Water-based pollution is one of the global challenges in the whole world. Every year a large amount of natural water resources is polluted by the discharge of toxic organic and inorganic pollutants from industries and domestic places. For instance dyes, pesticides and antibiotics are one of the most common organic pollutants present in wastewater [18]. These organic pollutants have adverse effects on the aquatic flora and fauna. Moreover, such organic pollutants may also cause serious threats to human beings, leading to cytotoxicity, cancer, skin diseases, etc. [19,20]. Antibiotics are mainly dumped into the water bodies from the pharmaceutical industries, hospitals, unused antibiotics from houses, etc. The antibiotics from these sources interact with the normal microflora of the environment and lead to antibiotic resistance [21]. Once the exposed microbes develop antibiotic resistance, it becomes very difficult for the patient during antibiotic therapy treatment. In order to prevent antibiotic resistance by microbes, these antibiotics must be treated by the industries much more efficiently by using a photocatalytic nanomaterial, such as ZnONPs. Earlier Zhou and their team have also shown the removal of antibiotics from swine wastewater by using anaerobic digestion as a strategic approach [22]. A team led by Hasan also showed the remediation of antibiotics from the wastewater. In addition to this, the investigators also showed the adverse effect of antibiotics on microbial communities [23]. Alameri and their team first developed activated carbon from *Azolla filiculoides* biomass, which was embedded with magnetic and ZnONPs, the size of the developed nanocomposite was 2.26 nm, and the surface area was $1401 \text{ m}^2 \text{ g}^{-1}$. Second, the developed NC was used for the removal of ciprofloxacin (CIP) from the wastewater and here, the removal efficiency of 100% within 1 h 15 min when the CIP concentration was 10 mg/L, having pH of 5 and temperature $30 \text{ }^\circ\text{C}$ [24]. Yilmaz and their group synthesized activated carbon (AC) from *Lemna minor* plant. The AC was then decorated with magnetite NPs. Furthermore, the developed NC was used for the removal of CIP antibiotics. Investigators reported 100% removal of CIP within 1 h and 15 min when the dose of the NC was 0.75 g/L [25]. Kyzas and their reported the ultrasound-mediated degradation of CIP by using ultrasound and ferrous ions-activated H_2O_2 and persulfate. The investigators obtained 100 percent removal of CIP within 50 min at pH 3 [26]. Balarack and their reported the removal of azithromycin from the wastewater by using porous AC obtained from *Azolla filiculoides*. Within a time period of 1 h 15 min, there was the removal of about 87% and 98% at 303 K and 333 K, respectively [27]. In all such approaches plant-mediated, AC was used directly or as supporting material for embedding different NPs, such as magnetite and ZnONPs, but no attempts were made the removal of antibiotics by using ZnONPs alone. Moreover, none of the above-mentioned has reported the removal of amoxicillin removal from the wastewater. Thus, the current approach is different from the previously reported method. Musawi and their team reported the removal of 99.3% of levofloxacin within 90 min by using nanocomposite (MWCNTs/CoFe₂O₄) [28].

With the continuously increasing population, there is a huge demand for textiles and clothes around the whole globe. Moreover, the biological laboratories use various stains and dyes which are finally drained into the sewer from where they are mixed with the nearby water bodies or microbes present in this aquatic system. Among the most widely used dyes in scientific laboratories are methylene blue [29–32], while in the textile aniline dyes, azo dyes, etc. These dyes are discharged into the water bodies leading to various harmful effects, which, in long term, may cause skin diseases and cancer [33]. Thus, there is a need to remediate these dyes, especially methylene blue dyes, which are commonly used in science laboratories and disposed of into the sewage system without treating it. Several

attempts were made by different investigators the removal of MB dye from wastewater or from simulated wastewater. For instance, Patel and their team emphasize the removal of textile dyes from wastewater by microbial approach [33]. Gnanamoorthy and their team also showed the potential of photocatalytic nanocomposites for the removal of MB dyes from wastewater [34]. In addition to this, Modi and their team showed the remediation of dyes from simulated wastewater by using ZnONPs [35]. Choudhary and their team also showed the MB dye removal from the river and effluent water by using nano clay [36].

Even though there are several techniques available for the remediation of organic pollutants from wastewater, such as adsorption, precipitation, coagulation, electroplating, sedimentation, flocculation, etc. However, the majority of these techniques are not only ineffective, but it generates harmful by-products which is a challenging issue. Thus, there is a need for a technology which completely mineralizes organic pollutants, such as antibiotics and methylene blue dye, without generating any byproducts. Thus, a photocatalytic nanoparticle [37], such as ZnONPs, is the based approach for remediation is the most effective method.

The present work emphasizes the ZnONPs synthesis by using the scallion's onion peel waste and observing the phytotoxicity of the synthesized zinc oxide nanoparticles on wheat saplings and antibiotic removal from simulated water. The synthesized ZnONPs were thoroughly analyzed by sophisticated instruments for detailed information about the particles. Finally, the objective was to observe the effect of various ppm dosages of ZnONPs on wheat sapling growth. Another objective of this work was to assess the potential of scallion-mediated synthesized ZnONPs for the remediation of antibiotics (ampicillin) from the simulated wastewater. Moreover, yet another objective was to assess the potential of scallion-mediated synthesized ZnONPs for the remediation of dye (methylene blue) from simulated wastewater. In addition to this, one more objective was to observe the photocatalytic effect of ZnONPs on the antibiotic and dye removal in the presence of UV and visible light.

Synthesis by such type of plant waste material could prove to be the economical, eco-friendly, and biocompatible approach. Moreover, such a type of approach will also minimize the solid waste that arises from the accumulation of peels generated from scallions and attracts flies and mosquitoes, which act as a vector for several diseases.

2. Materials and Methods

2.1. Materials

Zinc chloride (Sigma Aldrich, Germany, 98.9% AR grade), Ethanol (SRL, Gujarat, India), Sodium hydroxide pellets (SRL, Gujarat, India, 98%, Analytical grade), Ampicillin (Himedia, New Delhi, India, AR grade), Methylene blue dye (Chemall, New Delhi, India, AR grade), scallions' onion peel, and wheat seeds.

2.2. ZnONPs Synthesis by Using Scallions Peel Extract

2.2.1. Preparation of Scallion's Skin Extract

The scallion's onion peel was obtained and washed 2–3 times with distilled water to remove the large dirt and dust on its surface. The scallion's peel was dried in an oven and became a dry powder by using a blender (Japan: JP KKMKG 750-Watt), as shown in Figure 1. Since the grinding was non-homogenous, the powdered particles were sieved to remove larger particles. The fine powder was collected, and 10 g was taken and soaked in double distilled water (ddw) in a round bottom (RB) flask. About 100 mL (80%) ethanol was added to the RB flask and vigorous stirring was completed at 400–500 rpm along with heating at 60 °C for 20 min. After 20 min, the mixture was cooled to room temperature (RT). Furthermore, the reaction mixture was transferred to a falcon tube and centrifugation of the reaction mixture was completed at 7000 rpm for 5 min. The supernatant was collected while the residue was discarded. For the synthesis of ZnONPs, 50 mL of filtrate was taken. The qualitative and quantitative analysis of the scallion's onion peel extract was carried out by using standard methods [38].



Figure 1. (a) Photograph of scallion's onion and (b) dried peel from scallions.

2.2.2. Synthesis of ZnONPs

A 2 mM ZnCl_2 solution was prepared by mixing it with the 200 mL ddw, which was continuously kept stirring for 20 h on a magnetic stirrer. From the previous experiments performed by the author, standard parameters were followed, i.e., throughout the experiment pH was kept near 8 by using 1 M NaOH alkali solution. The aqueous solution of ZnCl_2 was shifted to a 250 mL round bottom flask (RBF), which was fitted with a reflux condenser. To, the aqueous solution of 2 mM ZnCl_2 about 30 mL of scallion's onion peel extract was poured dropwise. The mixture was continuously agitated along with rigorous stirring at 400–500 rpm and was observed for color change. After 30–35 min, there was a change in the color of the reaction solution and after that, the mixture was continuously stirred at 400–500 rpm for 4 h. Once the reaction was over, the mixture was transferred to a falcon tube and centrifugation was completed at 7000 rpm for 7 min to obtain the solid particles. Furthermore, the supernatant was decanted while the solid particles were mixed with ddw, and again, it was centrifuged. This process was repeated several times in order to remove any impurities present in the particles. Finally, after 2–3 washing, the solid particles were retained while the supernatant was discarded. Finally, the solid particles were transferred to a Petri plate and oven-dried at 70–80 °C till they dried completely. The dried powder was then calcinated at 400 °C in a muffle furnace (Patel Scientific, Ahmedabad, Gujarat, India) by increasing the temperature 5 °C per minute. The schematic diagram (Figure 2) shows the steps involved in the synthesis of ZnONPs by using scallion peel extract.

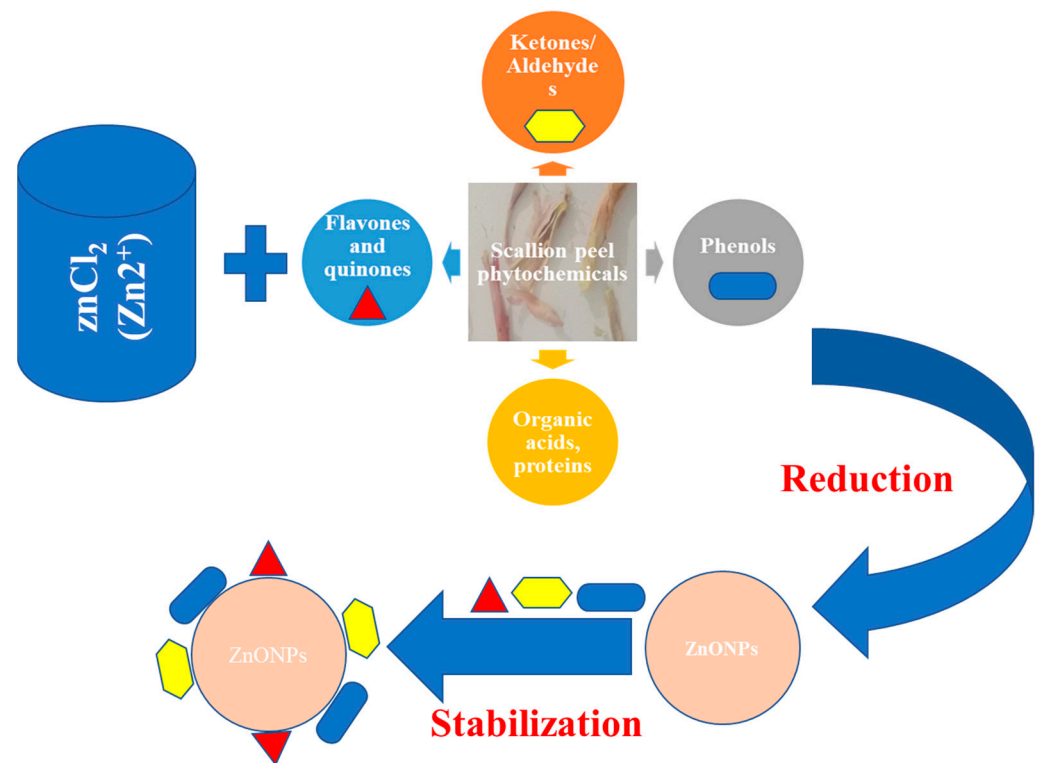


Figure 2. Schematic diagram for synthesis of ZnONPs using scallion peel extract.

2.2.3. Characterization of ZnONPs

In order to confirm that the ZnONPs were synthesized by using dried scallions peel extract, various analytical techniques were used. For UV-Vis analysis, a pinch of powder sample was added in ddw and sonicated for 10 min to disperse the samples. The samples were screened for 200 nm to 600 nm at a resolution of 1 nm. The analysis was done by an Agilent-made spectrophotometer (Carry win 60, Santa Clara, CA, USA). For morphological features field emission scanning electron microscope (FESEM) of Nova Nanosem, 450 FEI (The Netherlands) were used, while for the crystalline structure X-ray diffraction (XRD) was completed by using D-8 Advanced, Focus P-XRD, Bruker (Germany). The presence of various functional groups in the synthesized NPs was analyzed by Fourier transform-infrared spectroscopy (FTIR). FTIR measurements were completed in the range of $400\text{--}4000\text{ cm}^{-1}$, by using SP 65, Perkin Elmer, (Germany), at a resolution of one nm. The analysis was completed by preparing the KBr pellet method, where ZnONPs powder was mixed with KBr in a ratio of 2:198 mg. The thoroughly mixed mixture was then pressed with a mechanical press to obtain a disc of 1–2 cm. The particle size distribution of the sample is an important feature that was analyzed by using a particle size analyzer of the following made, Malvern, Zetasizer, S90 (USA). For analysis, 1–2 mg ZnONPs were taken in a 2 mL Eppendorf tube. The Eppendorf tubes were sonicated thoroughly for five minutes in an ultrasonicator (Sonar, 40 kHz). Furthermore, for average particle size measurement, approximately 1 mL dispersed sample was taken in the cuvette and measurements were performed at RT.

2.2.4. Phytotoxicity of the ZnONPs on the Plant Growth

Here, ZnONPs were synthesized by peel extract of scallions onion, which was further used as a micronutrient for the wheat plant. ZnONPs of the following ppm solution were prepared: 50, 150, 300, 600, 900, and 1200 ppm, respectively, of ZnONPs were prepared. The wheat seeds were purchased from a local vendor, then it was thoroughly washed with ddw at least 2–3 times and kept at RT. The procedure for studying phytotoxicity on the wheat plant was similar to the previous studies reported by Modi et al., where the phytotoxicity

on the wheat plant was observed but the synthesis of ZnONPs was varied out by using peels of onion collected from the vegetable market [11].

2.2.5. Seedling Exposure

The wheat seeds were suspended in the ddw in order to check their viability as the seeds that float at the top will not be used for the experimental study, while the seeds which settled at the bottom were further used. These settled seeds were further washed with ddw 2–3 times followed. Furthermore, these seeds were added to the ZnONPs aqueous mixture, which was kept under sonication for two hours for proper dispersion of the particles. Once the sonication was over after two hours the seeds were left undisturbed in the same solution overnight. After 24 h, the soaked seeds were taken out and placed in the respective earthen pots for the further effect of ZnONPs on plant growth [39].

2.2.6. Physico-Chemical Analysis of Soil

For the experimental analysis soil was collected from the University area (Gandhinagar, Gujarat). The soil was loamy sand, which was passed through sieve sets and used for physicochemical analysis.

2.2.7. Root and Shoot Length

Here, the length of the root was measured from the point below the hypocotyls to the end of the tip of the root, while the length of the shoot was taken from the cotyledon's base. For measuring both roots and shoot, a thread and a scale were used.

2.2.8. Seed Germination Test

The calculation of relative seed germination rate (RSG) and relative root growth (RRG) was completed by using the equation and germination index (GI).

$$\text{RSG Rate} = (S_c/S_s) \times 100$$

$$\text{RRG} = (R_s/R_c) \times 100$$

$$\text{GI} = (\text{RSG}/\text{RRG}) \times 100$$

In the above formula, S_s stands for the total number of germinated seeds in the sample, and S_c represents the total number of germinated seeds in the control. In addition to this, R_s represents the average root length in the sample and R_c represents the average root length in the control.

2.2.9. Fresh and Dry Weight

A weighing balance was used for measuring the fresh weight of both the root and shoot of seedlings separately. Once the fresh weight was taken for the seedlings, it was then transferred to a hot air oven at 60 °C for two days; after which their dry mass was measured.

2.2.10. Preparation of Ampicillin and Methylene Blue Aqueous Solution

About 500 mL of an aqueous solution of 400 ppm ampicillin and 300 ppm of methylene blue dye was prepared in double distilled in a separate volumetric flask, respectively. Furthermore, both samples were divided into 2 equal parts of 200 mL in a beaker for further experimental investigation. Figure 3a shows an image of Ampicillin, while Figure 3b is showing an image of methylene blue.

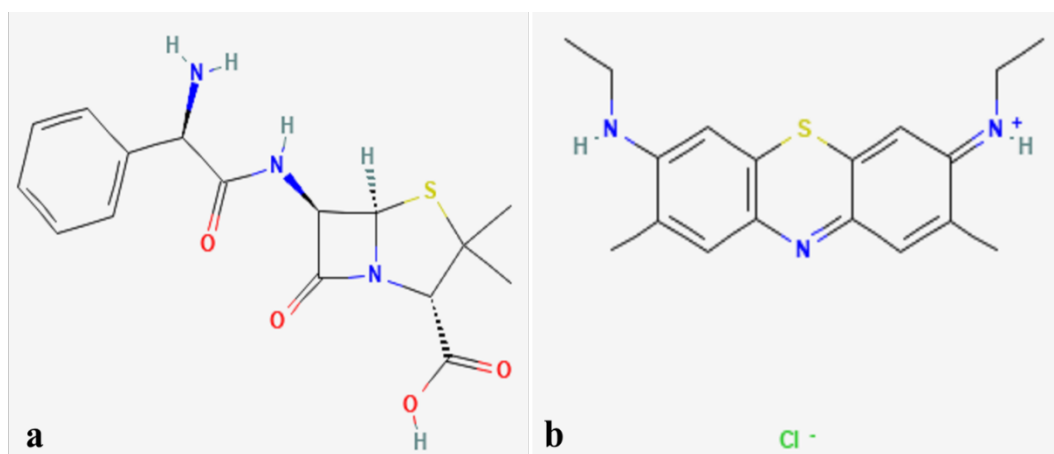


Figure 3. Molecular structure of (a) ampicillin and (b) methylene blue.

3. Results and Discussions

3.1. UV-Vis Measurement of Synthesized ZnONPs

UV-Vis is the basic technique for the preliminary investigation of the synthesized ZnONPs. Figure 4 shows a UV-Vis spectrum of ZnONPs synthesized by scallion peel extract. From the figure, it is clear that the UV has a peak at 380 nm for the synthesized ZnONPs. While in general, the peak for ZnONPs may fall in the range of 355–380 nm depending on the size and other features of the material. An earlier a team led by Shahmari also reported a band at 357 nm, which was attributed to the intrinsic band gap of Zn-O absorption [40]. A team led by Talam also obtained a UV-Vis band at 355 nm for the synthesized ZnONPs [41]. Iqbal and their team obtained a UV-Vis band at 399 nm, synthesized from *L. nobilis* leaf extract [13]. Fakhari and their team also obtained a band at 385 nm for the synthesis of ZnONPs [13]. Numerous investigators have also reported similar spectra in the range of 355–380 nm for ZnONPs, for instance Khan and their team [42–45].

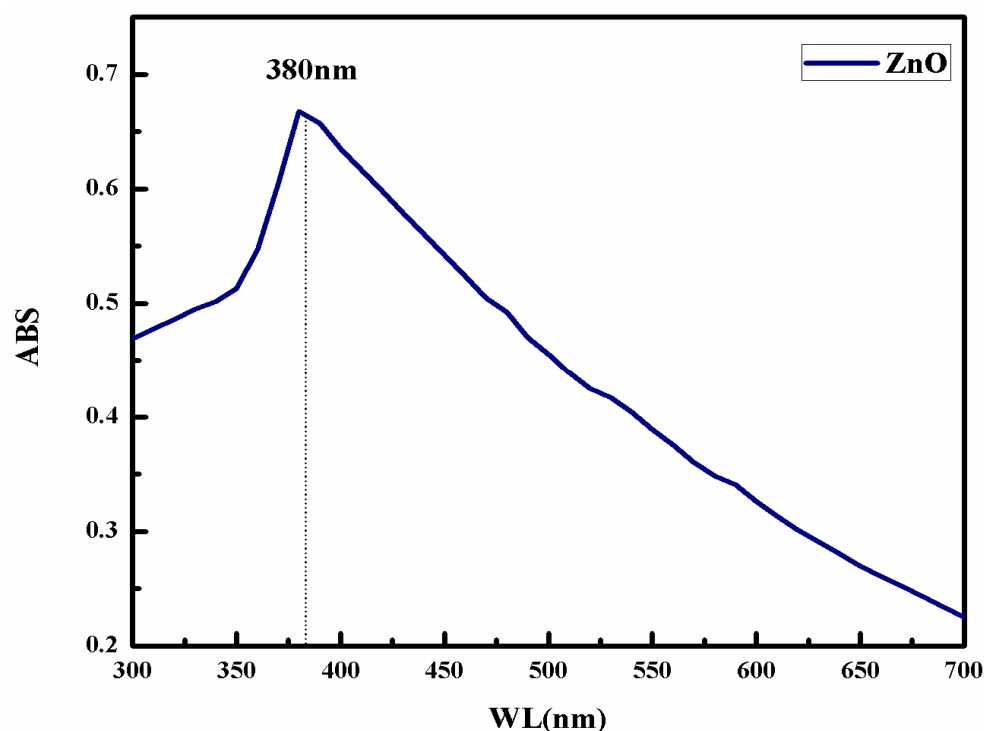


Figure 4. UV-Vis spectra of ZnONPs synthesized by scallions peel.

3.2. Microscopic Analysis of ZnONPs by FESEM and TEM

From Figure 5a, FESEM of ZnONPs, it is clearly visible that the particles are spherical and irregularly rod-shaped. Since no capping agent or surfactant was used, spherical particles are showing aggregation and their size is relatively increased. Figure 3a shows a FESEM image of ZnONPs at 1 micron where particle morphology is not differentiable. Moreover, particles are showing aggregation. Figure 5b shows the FESEM micrograph of ZnONPs at 200 nm resolution, where there are two types of particles: the majority of the particles are spherical shaped whose size is 40–100 nm, while a few of them are present as rod-shaped whose size is above 200 nm. Fakhari and team also obtained spherical to bullet-shaped particles which were synthesized by zinc acetate and zinc nitrate, respectively, which were showing aggregation. The investigators concluded that the agglomeration is due to the polarity and electrostatic attraction of ZnONPs. In addition to this, Madan and their team also obtained similar observations [13].

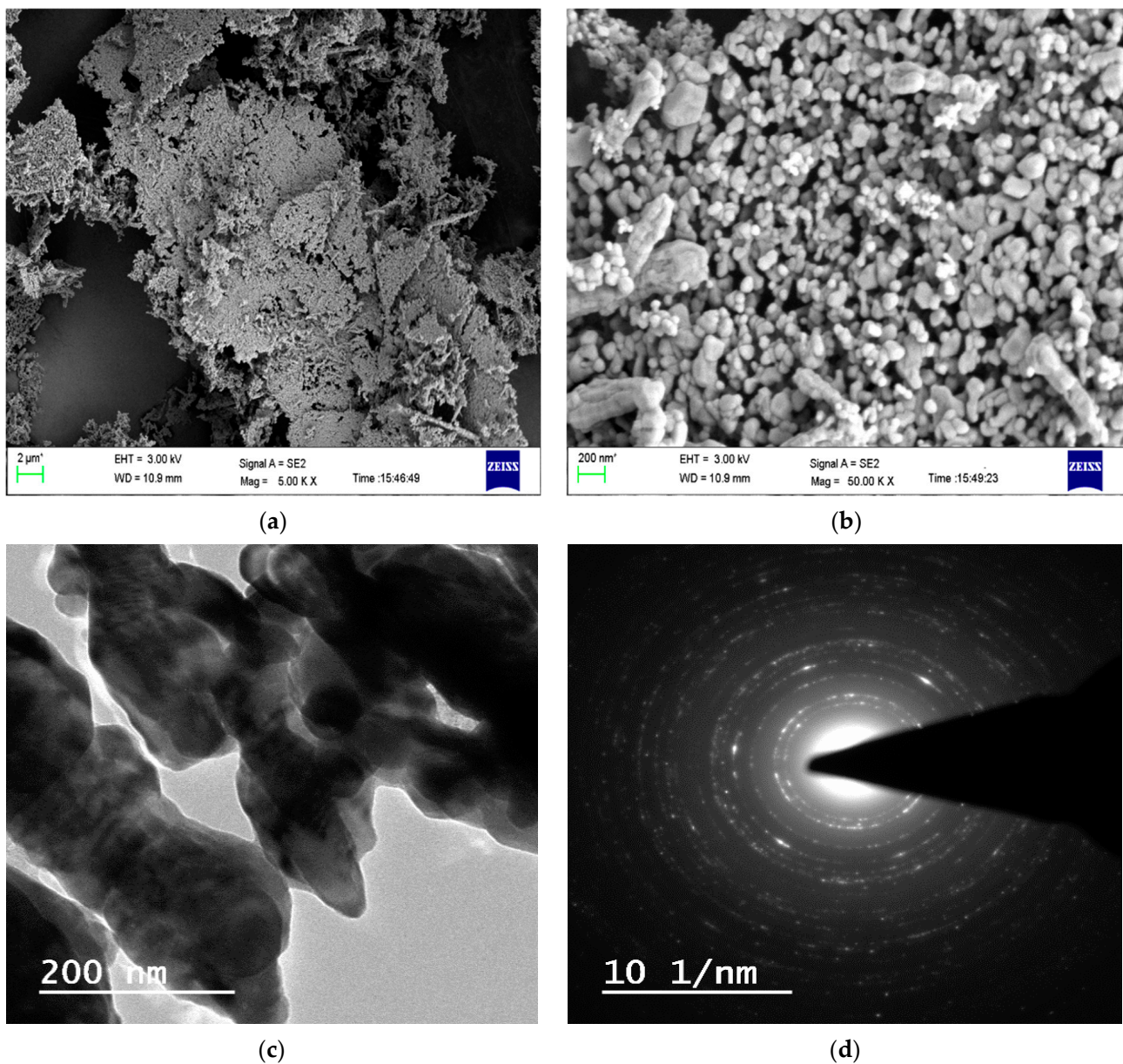


Figure 5. FESEM micrographs of ZnONPs (a) at 2 μm scale and (b) 200 nm synthesized by scallion's peel extract at 1 μm, TEM images of ZnONPs at 200 nm scale (c) and SAED pattern (d).

In addition to this, due to the drying and heating of the scallion's onion peel, most of the natural phytochemicals, such as flavonoids, terpenoids, etc. were reduced or transformed. Thus, these phytochemicals were not present for the capping of the NPs during synthesis which would have controlled the size of the synthesized ZnONPs. The second factor for the aggregation and large size of the particle is the calcination of the particles, which leads to the fusion of the ZnONPs at an elevated temperature. Additionally, the capping agent, which was present initially on the surface of the NPs, was lost during the calcination at 400 °C. Similar experiments were performed by Modi and their team obtained almost similar results. Here, the authors have synthesized ZnONPs from the dried onion peel waste. Earlier a few investigators also reported the aggregation of the plant-mediated synthesized ZnONPs, of which, one is Talodthaisong and their team and the second one was by Haque et al., 2020. The latter group used leaves extract of *Azadirachta indica* for the synthesis of ZnONPs. The obtained ZnONPs were hexagonal, spherical, and rod-like, which were highly agglomerated to form a large particle [46,47]. The results obtained were in agreement with Modi et al., 2022, by using *Allium cepa* peel [38]. Iqbal and their colleagues synthesized ZnONPs of average size ~26 nm.

While Figure 5c depicts the TEM image of synthesized ZnONPs at a 200 nm scale, which shows that there are two types of particles, i.e., one is spherical shaped whose size is below 200 nm (40–100 nm), while a few are more than 200 nm and are rod-shaped. The smaller and spherical particles are more dominant than the large irregular rod-shaped particles. The image also shows the aggregation of a few small spherical-shaped particles, whose reason is the calcination of the ZnONPs at a high temperature. Figure 5d shows the scattering area electron diffraction (SAED) pattern, which confirms that the obtained ZnONPs are crystalline in nature. Iqbal and their team reported ZnONPs of size ~26 nm from the leaf extracts of *Elaeagnus angustifolia* L. [12]. Khan et al., 2019 also observed similar results for the chemically synthesized ZnONPs where the investigators reported different morphology of ZnONPs by using a different type of Zinc precursor [45].

3.3. Particle Size Distribution (PSD) Pattern of ZnONPs by PSA

The PSD of the synthesized ZnONPs is exhibited in Figure 6. The graph clearly shows that the particle sizes are varied, but the average size of the ZnONPs is 200 nm in diameter. There are some particles whose size is even more than 200 nm, which is due to the second population species, i.e., rod-shaped particles. Additionally, there are a few agglomerated particles also which are contributing to the average size of the particles by PSA [47,48]. Since the PSA does not provide actual size rather it provides hydrodynamic size in comparison to FESEM and TEM, the size reported by PSA is larger than both the microscopic techniques. The results obtained here were close in resemblance with a team led by Modi [11], and Modi and Fulekar 2020, who synthesized ZnONPs by using onion peel waste and garlic peel waste, respectively. Recently, Iqbal and their team obtained a hydrodynamic size of about 205.9 nm, whose zeta potential was 13.8 mV along with a PDI of 0.132 [12].

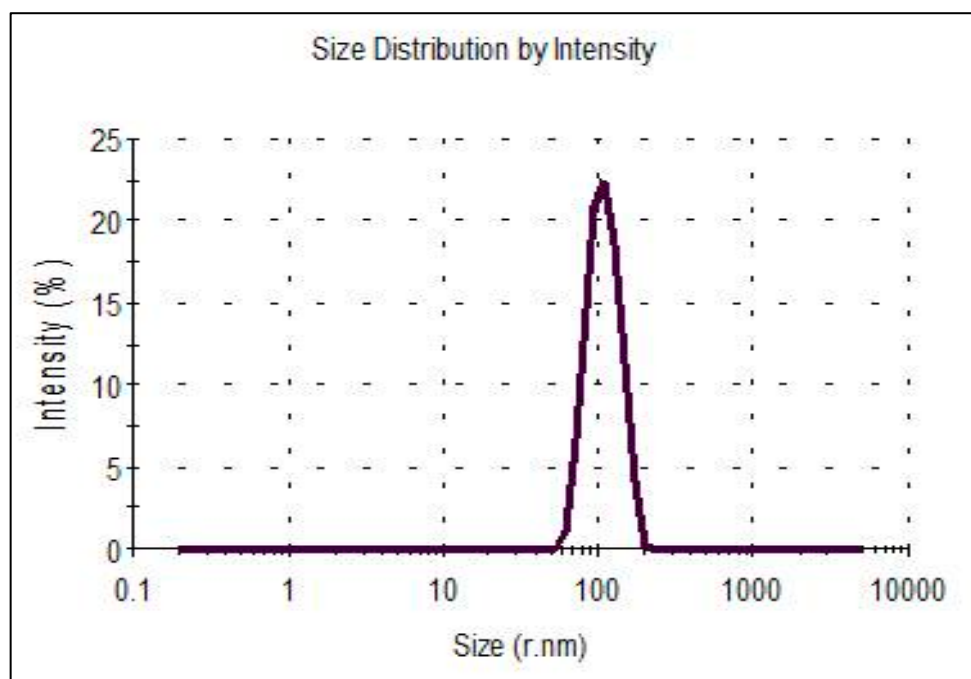


Figure 6. Particle size distribution of ZnONPs synthesized by scallion's peel extract.

3.4. Identification of Functional Groups of ZnONPs by FTIR

FTIR analysis was completed to find out the active bioactive compounds in the scallion's peel. Typical FTIR spectra of synthesized ZnONPs are shown in Figure 7, which have characteristic bands of ZnONPs at 510.3, 603.9, and 790.1 cm^{-1} . The bands from 400–800 are attributed to the weak and strong stretching vibrations of the Zn-O bond. The presence of bands in this region also confirms the formation of ZnONPs. Iqbal and their team also obtained a band at 498.25 cm^{-1} , which was attributed to the Zn-O stretching vibrations [12]. A band obtained at 1122.5 cm^{-1} is attributed to the C-O stretching and also due to the amide group in the synthesized ZnONPs, which was also obtained by Iqbal and their team at 1106.12 cm^{-1} . This particular group might be coming from the peel of scallions. In addition to this, a deep band at 1625.7 cm^{-1} is attributed to the C=O stretching. Moreover, this particular band could also be due to the (-OH) group in the ZnONPs. A small band near 2500 cm^{-1} is due to the atmospheric CO_2 adsorbed on the ZnONPs. A broad band at 3420.1 cm^{-1} is attributed to the (-OH) group present in the ZnONPs. The results obtained here were in close resemblance with earlier results obtained by Modi and Fulekar [38]. A team led by Rajendran and Beley have also obtained similar results for the chemically synthesized and green route synthesized, respectively [44,49]. Iqbal and their team also obtained a band at 3480.15 cm^{-1} , which was due to the alcohols and phenols of OH stretching [12].

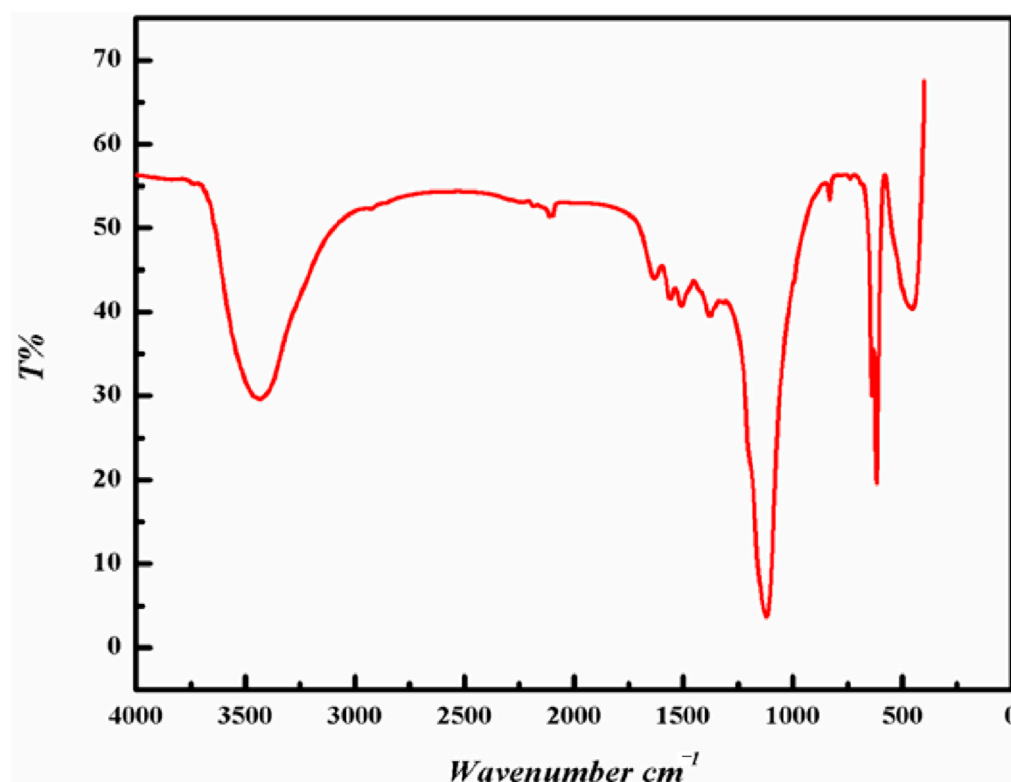


Figure 7. FTIR spectra of synthesized ZnONPs.

3.5. Thermogravimetric Analysis (TGA) and DSC Studies of ZnONPs

The thermal characters of ZnONPs were examined by the TGA, depicted in Figure 8a. The scallion peel mediated synthesized ZnONPs displayed a weight loss (reaction interval area) between ≈ 50 °C (initial temperature $\approx T_i$) and 574 °C (final temperature $\approx T_f$) due to the elimination of physically adsorbed water and the breakdown of organic/hydroxide components [50]. However, the TGA graph showed a descending trend in weight loss up to ≈ 574 °C may be due to the physically adsorbed organic molecules, while before ≈ 50 °C, there is no significant peak regarding weight-loss features. Rambabu and their group also observed the thermal stability of DP-ZnO-NPs with <10 wt% loss up to 700 °C, by using DSC/TG analysis [51]. The ZnONPs were of 30 nm size synthesized by Phoenix dactylifera waste. There is no significant variation in weight loss peaks in the TGA graph after ≈ 574 °C for as prepared ZnO as it is not functionalized with different chemical components [52]. The synthesized ZnO has its crystalline hexagonal geometry (confirmed by XRD), which is often considered a chemically stable phase. However, it is studied that the lightweight organic substances are adsorbed onto the stable ZnO surfaces. Therefore, the mass drop curve is clearly obtained by the organic degradation/decompositions while the ZnONPs remained stable with their lattice orientations, and hence, the mass drop does not start at 100% [53]. Figure 8b shows the DSC curve of the synthesized ZnONPs, which revealed endothermic peaks at around 285 °C. The broad peak at around 285 °C is probably due to the loss of chemically adsorbed volatile organic molecules and the formation of ZnONPs [54,55].

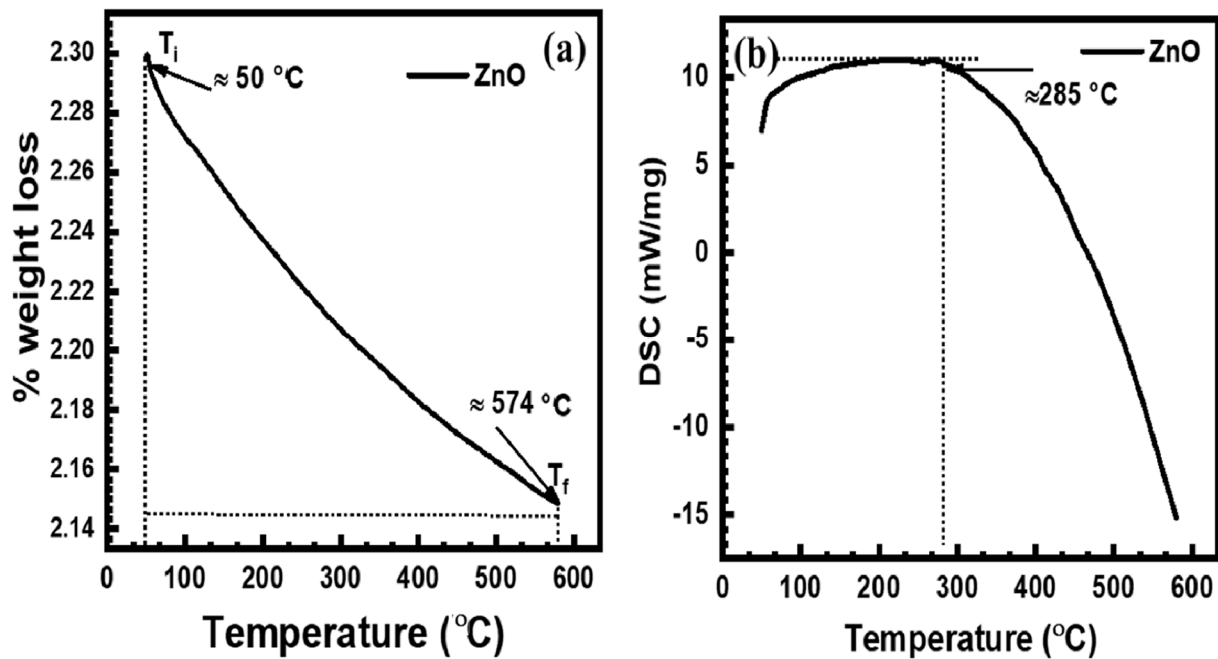


Figure 8. TGA (a) and DSC (b) analysis of ZnONPs synthesized by Scallion's peel.

3.6. Phase Identification of ZnONPs by XRD

The crystallinity and crystallite size of the ZnONPs were studied by using XRD analysis and the XRD profile is shown in Figure 9. The XRD characteristics peaks for the synthesized ZnO crystal particles are located at $2\theta = 31.50^\circ, 34.01^\circ, 36.07^\circ, 47.01^\circ, 56.34^\circ, 62.67^\circ, 66.01^\circ, 67.51^\circ, 69.22^\circ,$ and 76.91° correspond to the crystallographic planes of (100), (002), (101), (102), (110), (103), (200), (112), (201), and (202), respectively.

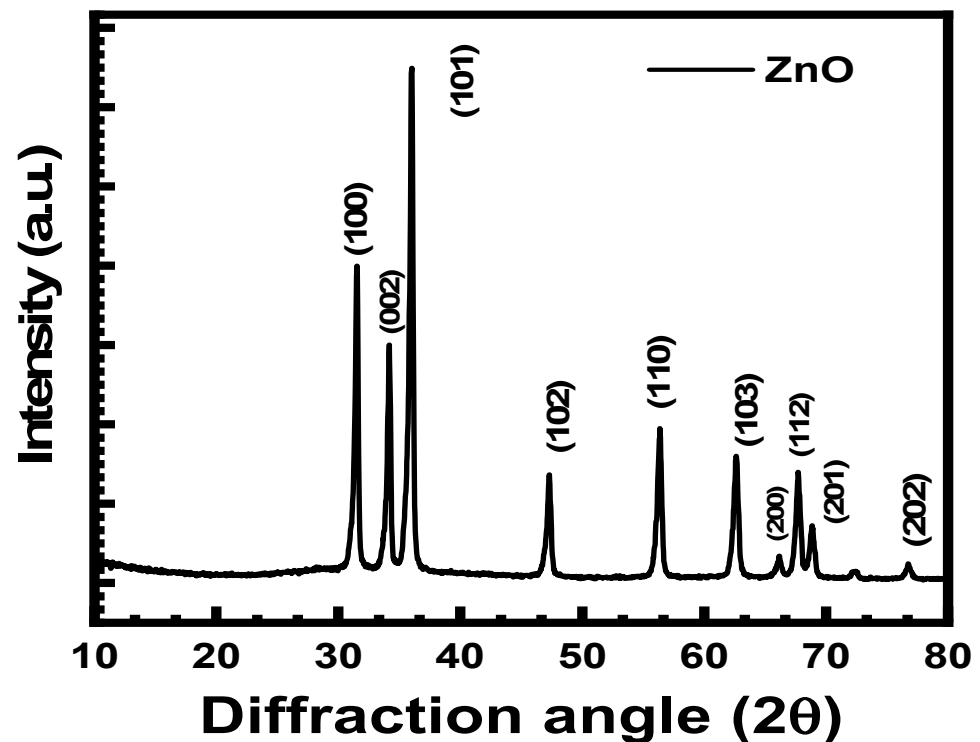


Figure 9. XRD profile of ZnONPs synthesized by scallion's peel.

The diffracted pattern of the XRD indicates a hexagonal crystalline geometry agreeing on the JCPDS card no. 01–007-2551. The average crystallite size of the ZnONPs was 42 nm as calculated by applying the Scherrer equation [24]. Iqbal and team also obtained peaks at 32.37 (100), 34.14 (002), 36.72 (101), 46.79 (102), 57.75 (110), 65.61 (103), 68.14 (112), and 69.94 (201) in the ZnONPs crystalline lattice. The investigators concluded the broader peaks in the synthesized XRD pattern are due to the small size of the ZnONPs [12]. Similar peaks were also reported by Modi and Fulekar 2020 [38], and Modi et al. 2022 [11] for the ZnONPs synthesized by the garlic peel extract and *Allium cepa* peel extract, respectively.

3.7. Physico-Chemical Analysis of the Soil Used

The soil which was used for the experimental studies was analyzed for its physico-chemical properties, for which the collected soil was analyzed for total nitrogen P, K, S, Zn, Fe, Mn, and Cu. Additionally, the collected soil was also screened for various physical parameters, such as conductivity and pH. The total N was about 0.87%, K was 3.65%, Mn (29.1%), and Cu (1.92%) were considered high. While P (5%), Zn (4.2 ppm), and Fe (8.4 ppm) were considered as low and medium, respectively. As far as conductivity and pH are concerned, pH is somewhat near neutral, i.e., 7.6, and conductivity is 1.35, which is directly associated with the ions. The results obtained with the wheat plants are shown in Table 1.

Table 1. Results for wheat saplings.

Treatment	Seed Germination %	Seedling Growth (cm)		Fresh Weight (g)		Dry Weight (g)	
		Root Length	Shoot Length	Root	Shoot	Root	Shoot
Control	45	6.29	9.31	0.042	0.211	0.0113	0.046
50 ppm	60	9.16	11.33	0.124	0.415	0.063	0.081
150 ppm	70	11.59	12.76	0.088	0.570	0.058	0.112
600 ppm	100	9.6	11.35	0.126	0.585	0.044	0.105
900 ppm	100	9.57	10.63	0.126	0.665	0.068	0.109
1200 ppm	65	8.46	9.56	0.074	0.434	0.049	0.071

3.8. Effect of Dosage of ZnONPs on the Seed Growth of the Wheat Plant

Figure 10 shows the various wheat seeds grown after different concentrations of ZnONPs. In the case of control seeds, the seed germination in wheat was noticed at just 45%, whereas an increase in the seed germination was noticed along with a gradual increase in the dosage (ppm) of ZnONPs.

At 50 ppm and 150 ppm, a 60% and 70% increase in the growth of seed germination was noticed, respectively. In addition to this, when the dosage of ZnONPs was 600 ppm, an increase in seed germination was noticed of about 100%. Furthermore, a decrease in seed germination was noticed for instance at 900 ppm, (100%) and at 1200 ppm (70%), respectively. Initially, low seed germination was noticed while using a lower dose of ZnONPs; after which, a slight increase in seed germination was observed with an increase in the dosage of ZnONPs. When the dosage of ZnONPs was higher, wheat plants started showing a phytotoxic effect which could be due to the heavy metal nature of Zn [56]. The ppm at which the wheat sapling showed maximum root length (11.59 cm) was 150 ppm of ZnONPs, and the least growth (6.29 cm) was noticed with the control sapling. As far as shoot length is concerned, the highest growth (12.76 cm) and lowest growth (9.31 cm) at 150 ppm and control, respectively. The ppm at which maximum fresh weight (0.126 g) of wheat plant root was obtained at 600 ppm and 900 ppm, while the lowest (0.042 g) was in the control plant. Whereas in the case of shoot weight, the highest was (0.665 g) and the lowest was (0.211 g) at 900 ppm and control, respectively. Among the dry weight of root, the highest was observed (0.068 g) and lowest (0.011 g) at 900 ppm and control, respectively while the highest weight of shoot highest was (0.112 g) and lowest (0.046 g) at 150 ppm and

control, respectively. Several investigators have also performed similar work and obtained close results for instance a team led by Adrees and Tondey separately concluded that zinc promotes wheat plant growth as it is an essential micronutrient. Moreover, investigators also concluded that if a high dosage of zinc is used as a micronutrient for the plant, then it may exhibit to phytotoxic effect [26]. As a result, delay in the growth of the plant will be observed, which will be visible in the form of short root or shoot length, wet weight, and dry weight [57,58].

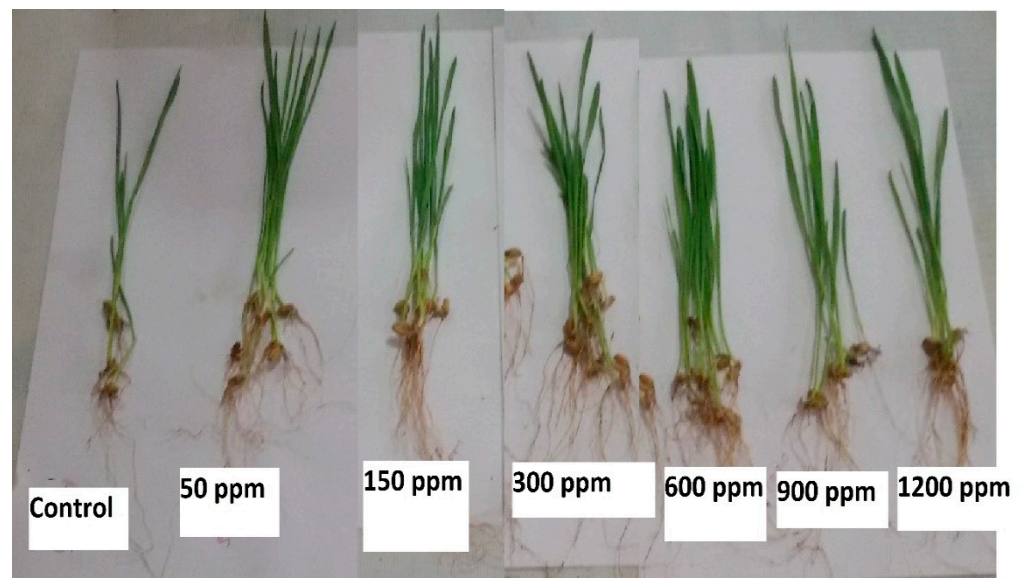


Figure 10. Growth of wheat seeds after treatment with different concentrations of ZnONPs.

4. Removal of Antibiotics and Dye from Wastewater under Visible and UV Light

4.1. Ampicillin Antibiotic Removal from Simulated Wastewater

For studying ampicillin removal from the simulated wastewater samples, about 200 mL of sample was taken in two separate beakers, to which 3 mg ZnONPs was added in each beaker. One beaker was kept in visible light while the other one was under UV light inside a laminar airflow (LAF) along with continuous stirring at 400 rpm with the help of a magnetic stirrer. An initial sample (at 0 min) was collected first for analysis. Furthermore, an aliquot was taken every 10 min to 1 h from both samples and analyzed by an Agilent-made spectrophotometer (Carry win 60, USA). The ampicillin has a maximum absorbance at ($\lambda_{max} = 207 \text{ nm}$), so the UV-Vis absorbance was taken at this particular wavelength.

From the UV analysis of dye removal under visible light, Figure 11a shows the initial sample the intensity was highest. Furthermore, there was slight a decrease in the peak intensity of the ampicillin from 10 min to 60 min. In addition to the peak of ampicillin, there were peaks of ZnONPs also in the samples as it was not filtered or centrifuged before the analysis of the samples.

The ZnONPs based ampicillin removal under UV light also shows that there was slight decrease in the intensity of antibiotic from 0 min to 60 min gradually. In addition to ampicillin peaks, there are several other prominent peaks which also might be due to the ZnONPs present in the samples and/or other components formed during the photocatalytic degradation of ampicillin. From Figure 11b, it is quite obvious that in the initial sample there was no other peaks except for ampicillin, but after that, the samples there were several large and small peaks, which indicates the degradation of the ampicillin into several other products with the increase in the contact time. The percentage degradation of the of ampicillin antibiotics from simulated wastewater was calculated by using this formula.

$$\text{Degradation percentage (\%)} = \frac{\text{Absorbance at zero time} - \text{absorbance at interval time}}{\text{bsorbance at zero time}} \times 100 \quad (1)$$

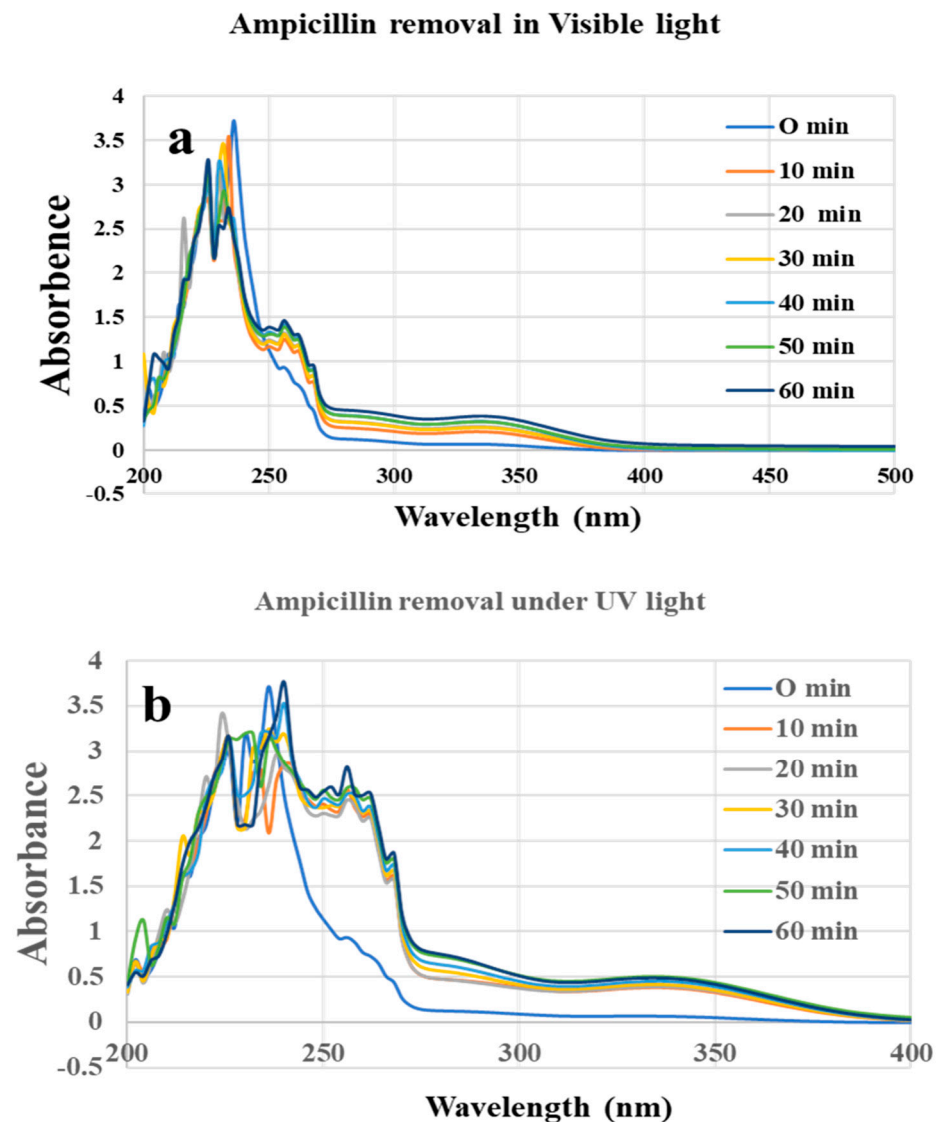


Figure 11. UV–Vis absorbance spectra of ampicillin antibiotic from simulated water under (a) visible light and (b) UV light with time by ZnONPs.

Previously several investigators also reported the nanoparticles-based remediation of several antibiotics from the wastewater, but only a few attempts were made for the ampicillin removal by using biologically synthesized ZnONPs. Zhou and their team remediated the antibiotics present in the swine wastewater in an anaerobic digester with enhanced efficiency [59]. Hassan and their team also summarized various approaches applied for the removal of antibiotics from wastewater [22]. Earlier, Chaba and their team also showed the remediation of amoxicillin from wastewater by using nanocomposite developed by carbon nanofibers coated zinc oxide. The investigators concluded that the developed nanocomposite exhibited maximum adsorption of amoxicillin when the dose of nanocomposite was 156 mg/g, and the kinetic study reveal that the adsorption method could be best described by pseudo-first-order reaction and the equilibrium data filled a Langmuir isotherm model [60]. Musawi and their team also reported the degradation of amoxicillin under UV light by using a nanocomposite ($\text{Fe}_2\text{O}_3/\text{bentonite}/\text{TiO}_2$ ($\text{Fe}_2\text{O}_3/\text{B}/\text{TiO}_2$)). The antibiotic was removed up to 100% within 60 min in UV light while 98.8% removal was seen under visible light [61]. Moreover, Musawi and their team removed the same antibiotic by using under UV light by using $\gamma\text{-Fe}_2\text{O}_3@\text{SiO}_2@\text{ZIF8-Ag}$. Here, the authors reported the 100% removal of amoxicillin within 60 min [26,62].

4.2. Methylene Blue Dye Removal from Simulated Wastewater

For studying the MB dye removal by using a photocatalyst, about 3 mg ZnONPs were added in 2 separate beakers having 200 mL of MB dye. One beaker was kept in visible light while the other one was under UV light (Philips 22W) inside a laminar airflow (LAF), under continuous stirring at 400 rpm by using a magnetic stirrer. An initial sample (at 0 min) was collected first for analysis. Furthermore, an aliquot was taken every 10 min to 60 min from both samples and analyzed by a UV-Vis spectrophotometer. The MB dye in distilled water has a maximum absorbance at ($\lambda_{\max} = 665 \text{ nm}$), so the UV-Vis absorbance was taken at this particular wavelength [63].

Initially, there was a strong intensity peak for the methylene blue dye at 665 nm, which gradually decreased with respect to time (0 min to 60 min) as evident from Figure 12a. The intensity of the peak gradually decreased from 0 min to 30 min; after which, the peak intensity increased. From Figure 12a, it is clear that the least concentration of methylene blue has reached after 30 min; after which, the concentration of dye increased in the sample. This could be due to the ZnONPs that might have reached equilibrium; after which, desorption started to occur.

Figure 12b indicates the methylene blue dye removal under UV light. From Figure 12b, it is clear that the highest intensity peak was at 0 min and there was a sudden decrease in the intensity of the peak at 10 min. After 10 min, the intensity of the peak reached much lower indicating the removal of the majority of the MB dye under UV light. The lowest intensity was obtained at 50 min; after which, there was a slight increase in the intensity of MB dye.

Previously several investigators have also remediated the MB dye from the wastewater or from simulated water by using ZnONPs as nano photocatalysts under visible and UV light. For instance, Nguyen and Nguyen 2020 reported the removal of MB dye from wastewater by using ZnONPs synthesized at different temperatures (450 °C, 550 °C, 650 °C, and 750 °C, respectively) by thermal decomposition method. The investigators observed that after 40 min about 99% MB dye was removed under UV light. The photocatalytic degradation of MB dye followed a first-order reaction [64]. Here, both investigators also assessed the nano photocatalyst for their reusability. Fouda and their colleagues synthesized 3–33 nm ZnONPs by using marine green macroalgae, *Ulva fasciata*. Furthermore, the investigators used the ZnONPs for the removal of MB dye under dark and visible light conditions. Moreover, the materials were also used for the antimicrobial activity and reusability cycle of ZnONPs. The investigators showed that the maximum dye removal percentage was $(84.9 \pm 1.2\%)$ after 2 h 20 min when the dosage of ZnONPs was 1.0 mg mL^{-1} , at 7 pH and at 35 °C under UV light. Moreover, the removal percentage of MB dye was only $53.4 \pm 0.7\%$ in dark conditions under similar parameters [65]. In another experiment, Fouda and their team developed 10–55 nm sized nanocomposites from the varying concentration of copper oxide NPs and ZnONPs, synthesized by using biomass filtrate of *Penicillium corylophilum* As-1 (fungus). Investigators concluded that when the concentration of Zn was increased in the nanocomposite, the size of the nanocomposite also increased. The maximum MB dye removal obtained was 97% after 1 h and 25 min by using CuO/ZnO_{20/80} nanocomposite [66]. Patwa and their group synthesized ~250 nm ZnONPs by using fresh lemon juice and zinc acetate. The size of the ZnONPs was confirmed by using diffraction light scattering (DLS). The authors observed a 25% reduction in MB dye under UV light within 30 min. Khasay and their group synthesized ZnONPs, from an aqueous leaf extract of *Dolichos Lablab* L. (source of reducing and capping agent), of average particle size 29 nm. The investigators removed MB dye along with rhodamine B and orange II under visible and near UV light. The MB dye was removed up to 80% at 11 pH in 210 min [67]. Rambabu and their group synthesized ZnONPs of a mean size of 30 nm by using *Phoenix dactylifera* waste. The removal percentage of MB dye was about 90% [51]. Table 2 shows various biological synthesized ZnONPs and their application for removal of MB dye under UV-light.

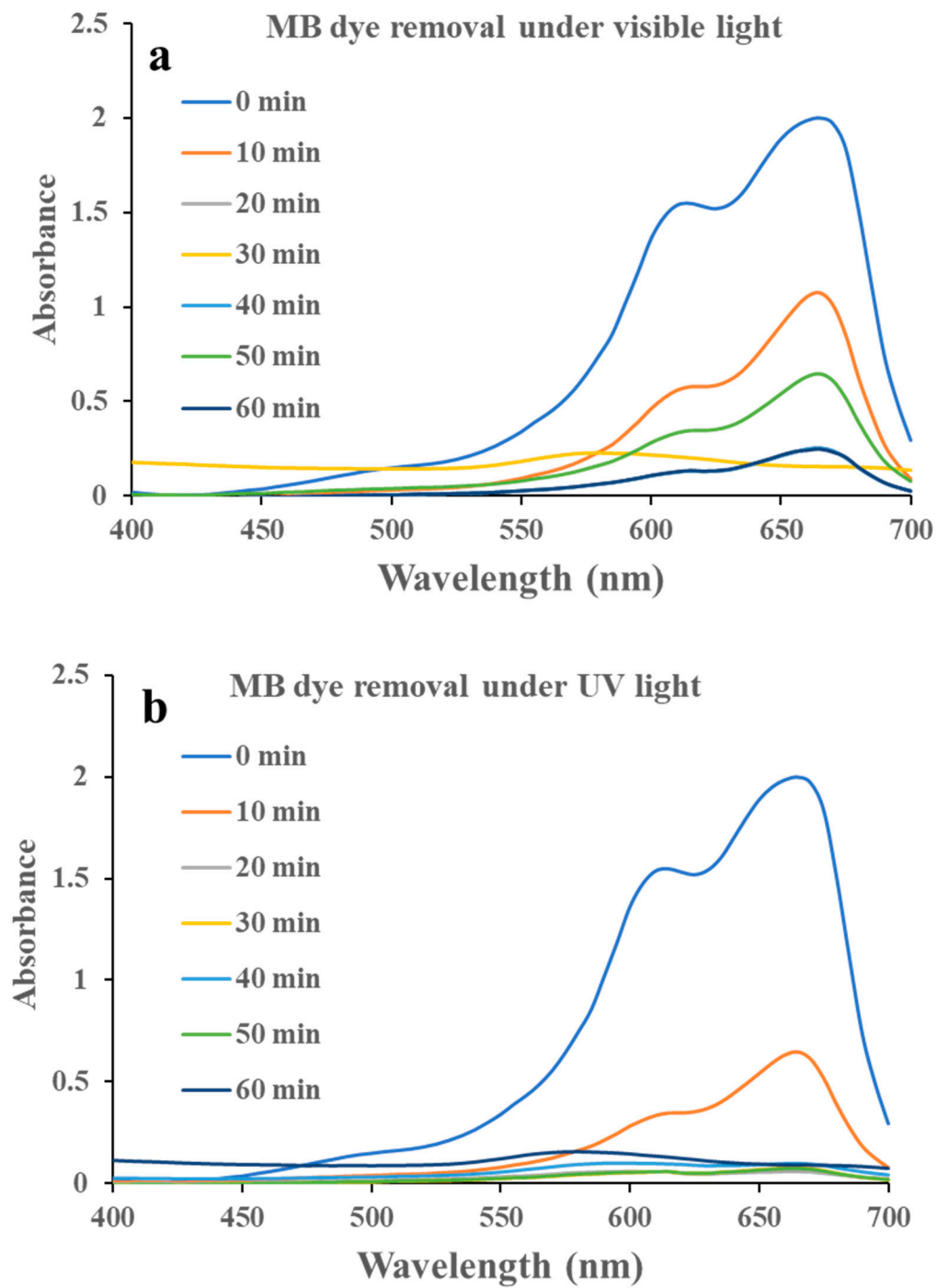


Figure 12. UV–Vis absorbance spectra of methylene blue dye from simulated water under (a) visible light and (b) UV light with time by ZnONPs.

Table 2. Photocatalytic degradation of MB dye by using plant and microbe-assisted ZnONPs under UV light and solar irradiation.

ZnO Photocatalyst	Precursor	Plant/Microbe Used	Size and Shape	Synthesis Method	Dosage of Phtocatalyst	Percentage Removal	Degradation Rate/Time	Ref.
ZnONPs				TD		99	40	[64]
		<i>Ulva fasciata</i>	3–33 nm	Phyco-assisted	1.0 mg mL ⁻¹	~85	140	[65]
CuO-ZnONPs NC		<i>Penicillium corylophilum</i> As-1	10–55 nm			97%	85	[66]
ZnONPs		<i>Phoenix dactylifera</i> waste	30 nm			90%		[51]
ZnO NPs	Zn acetate		29 nm		1 g L ⁻¹	80%	210 min	
ZnO cubes		Fresh lemon juice	Hexagonal rods (250 nm width and 1000 nm length), Cubes (250 nm)	Sol gel	-	25%	30 min	[68]
ZnO flowers	Zn nitrate	<i>Codonopsis lacceolata</i> root (Co-precipitation)	Flower, 500 nm			90.3%	40 min	[69]
ZnONPs	Zn nitrate	<i>Camelia sinesis</i> leaves	Sphere 8 mm			55–99%		
ZnO NPs		Garlic peel extract (GPE)	Rod and hexagonal 7.77 nm	Chemical-precipitation		65.8 (10 ppm)		[70]
ZnO/crystalline nanocellulose nanocomposite		GPE	59.51 nm	Chemical-precipitation		88.82 (10 ppm)		[70]
ZnONPs	Zinc nitrate					90.5%	180 min	
Spherical ZnONPs	ZnCl ₂	Scallion peel	50–90 nm	Chemical co-precipitation				This study

5. Dye Removal Mechanism

Here, in the present study, the UV light-based photocatalytic degradation showed better results for MB dye removal in comparison to visible light. The UV-light-based remediation of MB dye involved various phenomena, such as photoexcitation and separation, and hence, migration of charges from the valence band (VB) to the conductance band (CB) of nano photocatalyst. In addition to these events, there is also a surface oxidation-reduction process [66,71]. In the presence of UV light, the surface of ZnONPs is struck by photons ($h\nu$) of light, which is almost equal to or more than the BG of ZnO. Consequently, there is the excitation of electrons, which forms electron–hole pairs. From these electron-hole pairs; the former is transferred to the VB while the latter is transferred to CB as shown in the equation. Equation (2). The electrons, which are generated over here, are carried to the surface of the ZnONPs, which are involved in the redox reactions. The h^+ on the VB interacts with the H₂O or OH (hydroxide ions) forming \bullet OH (hydroxyl radicals), according to equation (III). The electrons present on the CB react with the O₂ molecule and form superoxide anion radical (\bullet O²⁻). This event is followed by the production of hydrogen peroxide (H₂O₂), according to Equations (4)–(6). In the last step, the produced radical species reacts with MB dye and transforms into intermediate products that will be hydrolyzed into harmless products (i.e., CO₂ and H₂O) according to Equation (7) [72,73] Figure 13



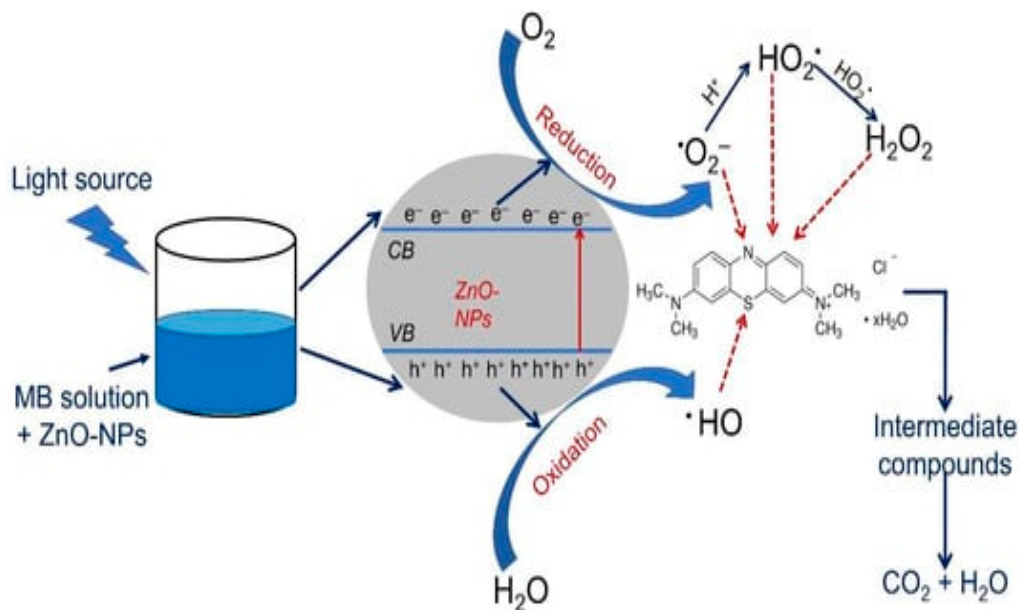
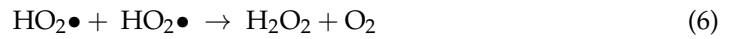
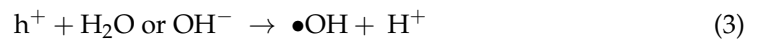


Figure 13. Mechanism of photocatalytic degradation of MB dye under UV-light adapted from.

6. Conclusions

There are several elements and their oxides that act as important nutrients for the developing plants, but its excess quantity may lead to the toxicity to the plant. Zinc and zinc oxide nanoparticles are essential nutrients required for various metabolic activities. Zinc oxide nanoparticles synthesized by biological routes, such as a plant, could solve the problem of biocompatibility since the plant extract acts as a source of capping agents. The ZnONPs synthesized by scallion's peel were of size 40–100 nm (spherical-shaped) and above 200 nm (rod-shaped), which have several functional groups as confirmed by the FTIR. It was found that ZnONPs enhance the growth of seeds up to certain dosages; after which, the concentration of element reaches a toxic level and affects the plant. The obtained results show that ZnONPs at lower to high dose increases seedling growth, seed germination percentage, and fresh and dry weight indicating that the dose of ZnONPs up to 600 ppm is not toxic for wheat plants. Both antibiotic and methylene blue dye removal study was carried out under visible and UV-light for one hour. The remediation study found that remediation of both ampicillin and methylene blue dye was efficient under UV light under similar reaction parameters from the simulated wastewater by the ZnONPs. Thus, it is possible to utilize scallion for the green synthesis of ZnONPs and could apply them for the remediation of ampicillin and methylene blue dyes under visible and UV light effectively and efficiently in simulated and wastewater water.

Author Contributions: Conceptualization, S.S., H.A., V.K.Y., S.M., A.P. (Ashish Patel) and N.C.; Data curation, V.K.Y., S.S., K.K.Y., A.G. and S.H.K.; methodology, S.S., H.A., M.M.S.C.-P., S.M. and S.H.K.; validation, K.K.Y., S.M., M.M.S.C.-P. and V.K.Y.; formal analysis, A.P. (Ashish Patel), S.H.K., V.K.Y., H.A. and A.G.; resources, K.K.Y., A.P. (Aradhana Patel), M.M.S.C.-P. and S.H.K.; writing—original draft preparation, S.S., V.K.Y., K.K.Y., N.C., S.M., A.P. (Aradhana Patel), M.M.S.C.-P. and A.G.,

writing—review and editing, N.C., H.A., V.K.Y., S.M., A.G., N.C., M.M.S.C.-P. and S.H.K.; supervision, V.K.Y., K.K.Y., A.G., N.C. and V.K.Y.; project administration, V.K.Y., K.K.Y. and A.P. (Ashish Patel); Funding acquisition, A.P. (Ashish Patel); H.A., A.G., S.S. and M.M.S.C.-P.; Investigation, A.P. (Ashish Patel), N.C., V.K.Y. and S.H.K.; Software's, K.K.Y., M.M.S.C.-P. and N.C.; Visualization, S.S., V.K.Y. and A.P. (Aradhana Patel). All authors have read and agreed to the published version of the manuscript.

Funding: Researchers Supporting Project number (RSPD2023R604), King Saud University, Riyadh, Saudi Arabia.

Institutional Review Board Statement: Not applicable.

Informed Consent Statement: Not applicable.

Data Availability Statement: All relevant data are included within the article.

Conflicts of Interest: All authors declare that there is no conflict of interest.

References

1. Yadav, V.K.; Gnanamoorthy, G.; Ali, D.; Bera, S.P.; Roy, A.; Kumar, G.; Choudhary, N.; Kalasariya, H.; Basnet, A. Cytotoxicity, Removal of Congo Red Dye in Aqueous Solution Using Synthesized Amorphous Iron Oxide Nanoparticles from Incense Sticks Ash Waste. *J. Nanomater.* **2022**, *2022*, 5949595. [\[CrossRef\]](#)
2. Khayal, A.; Dawane, V.; Amin, M.A.; Tirth, V.; Yadav, V.K.; Algahtani, A.; Khan, S.H.; Islam, S.; Yadav, K.K.; Jeon, B.-H. Advances in the methods for the synthesis of carbon dots and their emerging applications. *Polymers* **2021**, *13*, 3190. [\[CrossRef\]](#)
3. Spoială, A.; Ilie, C.-I.; Truşcă, R.-D.; Oprea, O.-C.; Surdu, V.-A.; Vasile, B.; Ficai, A.; Ficai, D.; Andronescu, E.; Diţu, L.-M. Zinc oxide nanoparticles for water purification. *Materials* **2021**, *14*, 4747. [\[CrossRef\]](#) [\[PubMed\]](#)
4. Al-Mamun, R.; Hasan, R.; Ahommed, S.; Bacchu, S.; Ali, R.; Khan, Z.H. Nanofertilizers towards sustainable agriculture and environment. *Environ. Technol. Innov.* **2021**, *23*, 101658. [\[CrossRef\]](#)
5. Verma, P.; Madamwar, D. Production of ligninolytic enzymes for dye decolorization by cocultivation of white-rot fungi *Pleurotus ostreatus* and *Phanerochaete chrysosporium* under solid-state fermentation. *Appl. Biochem. Biotechnol.* **2002**, *102*, 109–118. [\[CrossRef\]](#) [\[PubMed\]](#)
6. Khan, S.H.; Pathak, B. Zinc oxide based photocatalytic degradation of persistent pesticides: A comprehensive review. *Environ. Nanotechnol. Monit. Manag.* **2020**, *13*, 100290. [\[CrossRef\]](#)
7. Demissie, M.G.; Sabir, F.K.; Edossa, G.D.; Gonfa, B.A. Synthesis of Zinc Oxide Nanoparticles Using Leaf Extract of *Lippia adoensis* (Koseret) and Evaluation of Its Antibacterial Activity. *J. Chem.* **2020**, *2020*, 7459042. [\[CrossRef\]](#)
8. Naseer, M.; Aslam, U.; Khalid, B.; Chen, B. Green route to synthesize Zinc Oxide Nanoparticles using leaf extracts of *Cassia fistula* and *Melia azadarach* and their antibacterial potential. *Sci. Rep.* **2020**, *10*, 9055. [\[CrossRef\]](#) [\[PubMed\]](#)
9. Ameen, F.; Alsamhary, K.; Alabdullatif, J.A.; Alnadhari, S. A review on metal-based nanoparticles and their toxicity to beneficial soil bacteria and fungi. *Ecotoxicol. Environ. Saf.* **2021**, *213*, 112027. [\[CrossRef\]](#)
10. Alamdari, S.; Ghamsari, M.S.; Lee, C.; Han, W.; Park, H.-H.; Tafreshi, M.J.; Afarideh, H.; Ara, M.H.M. Preparation and characterization of zinc oxide nanoparticles using leaf extract of *sambucus ebulus*. *Appl. Sci.* **2020**, *10*, 3620. [\[CrossRef\]](#)
11. Modi, S.; Yadav, V.K.; Choudhary, N.; Alswieleh, A.M.; Sharma, A.K.; Bhardwaj, A.K.; Khan, S.H.; Yadav, K.K.; Cheon, J.-K.; Jeon, B.-H. Onion Peel Waste Mediated-Green Synthesis of Zinc Oxide Nanoparticles and Their Phytotoxicity on Mung Bean and Wheat Plant Growth. *Materials* **2022**, *15*, 2393. [\[CrossRef\]](#)
12. Iqbal, J.; Abbasi, B.A.; Yaseen, T.; Zahra, S.A.; Shahbaz, A.; Shah, S.A.; Uddin, S.; Ma, X.; Raouf, B.; Kanwal, S.; et al. Green synthesis of zinc oxide nanoparticles using *Elaeagnus angustifolia* L. leaf extracts and their multiple in vitro biological applications. *Sci. Rep.* **2021**, *11*, 20988. [\[CrossRef\]](#)
13. Fakhari, S.; Jamzad, M.; Kabiri Fard, H. Green synthesis of zinc oxide nanoparticles: A comparison. *Green Chem. Lett. Rev.* **2019**, *12*, 19–24. [\[CrossRef\]](#)
14. Usman, M.; Farooq, M.; Wakeel, A.; Nawaz, A.; Alam Cheema, S.A.; Rehman, H.U.; Ashraf, I.; Sanaullah, M. Nanotechnology in agriculture: Current status, challenges and future opportunities. *Sci. Total Environ.* **2020**, *721*, 137778. [\[CrossRef\]](#) [\[PubMed\]](#)
15. Li, C.; Song, B.-Y.; Teng, Y.; Zhang, X.-F.; Deng, Z.-P.; Xu, Y.-M.; Huo, L.-H.; Gao, S. Biomass-derived hierarchical porous ZnO microtubules for highly selective detection of ppb-level nitric oxide at low temperature. *Sens. Actuators B Chem.* **2021**, *333*, 129627. [\[CrossRef\]](#)
16. Mansour, A.T.; Alprol, A.E.; Khedawy, M.; Abualnaja, K.M.; Shalaby, T.A.; Rayan, G.; Ramadan, K.M.A.; Ashour, M. Green Synthesis of Zinc Oxide Nanoparticles Using Red Seaweed for the Elimination of Organic Toxic Dye from an Aqueous Solution. *Materials* **2022**, *15*, 5169. [\[CrossRef\]](#)
17. Rajendran, S.; Wanale, S.G.; Gacem, A.; Yadav, V.K.; Ahmed, I.A.; Algethami, J.S.; Kakodiya, S.D.; Modi, T.; Alsuhaibani, A.M.; Yadav, K.K.; et al. Nanostructured Iron Oxides: Structural, Optical, Magnetic, and Adsorption Characteristics for Cleaning Industrial Effluents. *Crystals* **2023**, *13*, 472. [\[CrossRef\]](#)

18. Mallikarjunaswamy, C.; Parameswara, P.; Pramila, S.; Nagaraju, G.; Deepakumari, H.N.; Ranganatha, V.L. Green and facile synthesis of zinc oxide nanoparticles for enhanced photocatalytic organic pollutant degradation. *J. Mater. Sci. Mater. Electron.* **2022**, *33*, 20361–20372. [[CrossRef](#)]
19. Adegoke, O.R.; Oyewole, R.O.; Lasisi, B.M.; Bello, O.S. Abatement of organic pollutants using fly ash based adsorbents. *Water Sci. Technol.* **2017**, *76*, 2580–2592. [[CrossRef](#)] [[PubMed](#)]
20. Rawat, K. Organic pollutants in wastewater and its remediation approaches using graphene adsorbent. *Int. J. Agric. Appl. Sci.* **2021**, *2*, 8–13. [[CrossRef](#)]
21. Hassan, M.; Zhu, G.; Lu, Y.-Z.; Al-Falahi, A.H.; Lu, Y.; Huang, S.; Wan, Z. Removal of antibiotics from wastewater and its problematic effects on microbial communities by bioelectrochemical technology: Current knowledge and future perspectives. *Environ. Eng. Res.* **2020**, *26*, 190405. [[CrossRef](#)]
22. Yadav, V.K.; Amari, A.; Gacem, A.; Elboughdiri, N.; Eltayeb, L.B.; Fulekar, M.H. Treatment of Fly-Ash-Contaminated Wastewater Loaded with Heavy Metals by Using Fly-Ash-Synthesized Iron Oxide Nanoparticles. *Water* **2023**, *15*, 908. [[CrossRef](#)]
23. Zhou, Q.; Li, X.; Wu, S.; Zhong, Y.; Yang, C. Enhanced Strategies for Antibiotic Removal from Swine Wastewater in Anaerobic Digestion. *Trends Biotechnol.* **2020**, *39*, 8–11. [[CrossRef](#)] [[PubMed](#)]
24. Alameri, A.A.; Alfilh, R.H.C.; Awad, S.A.; Zaman, G.S.; Al-Musawi, T.J.; Joybari, M.M.; Balarak, D.; McKay, G. Ciprofloxacin adsorption using magnetic and ZnO nanoparticles supported activated carbon derived from *Azolla filiculoides* biomass. *Biomass-Converts. Biorefinery* **2022**, 1–14. [[CrossRef](#)]
25. Yilmaz, M.; Al-Musawi, T.J.; Saloot, M.K.; Khatibi, A.D.; Baniyadi, M.; Balarak, D. Synthesis of activated carbon from *Lemna* minor plant and magnetized with iron (III) oxide magnetic nanoparticles and its application in removal of Ciprofloxacin. *Biomass-Converts. Biorefinery* **2022**. [[CrossRef](#)]
26. Kyzas, G.Z.; Mengelizadeh, N.; Saloot, M.K.; Mohebi, S.; Balarak, D. Sonochemical degradation of ciprofloxacin by hydrogen peroxide and persulfate activated by ultrasound and ferrous ions. *Colloids Surfaces A Physicochem. Eng. Asp.* **2022**, *642*, 128627. [[CrossRef](#)]
27. Balarak, D.; Mahvi, A.H.; Shahbaksh, S.; Wahab, A.; Abdala, A. Adsorptive removal of azithromycin antibiotic from aqueous solution by *azolla filiculoides*-based activated porous carbon. *Nanomaterials* **2021**, *11*, 3281. [[CrossRef](#)]
28. Levofloxacin, D.; Hu, B.; Yang, L.; Al-Musawi, T.J.; Qasim Almajidi, Y.; Al-Essa, E.M.; Romero-Parra, R.M.; Alwaily, E.R.; Mengelizadeh, N.; Ganji, F.; et al. Levofloxacin Adsorption onto MWCNTs/CoFe₂O₄ Nanocomposites: Mechanism, and Modeling Using Non-Linear Kinetics and Isotherm Equations. *Magnetochemistry* **2022**, *9*, 9. [[CrossRef](#)]
29. El-Azazy, M.; El-Shafie, A.S.; Yousef, B.A.-S. Green tea waste as an efficient adsorbent for methylene blue: Structuring of a novel adsorbent using full factorial design. *Molecules* **2021**, *26*, 6138. [[CrossRef](#)]
30. Tsade Kara, H.; Anshebo, S.T.; Sabir, F.K.; Adam Workineh, G. Removal of Methylene Blue Dye from Wastewater Using Periodiated Modified Nanocellulose. *Int. J. Chem. Eng.* **2021**, *2021*, 9965452. [[CrossRef](#)]
31. Mir, I.A.; Singh, I.; Birajdar, B.; Rawat, K. A Facile Platform for Photocatalytic Reduction of Methylene Blue Dye by CdSe-TiO₂ Nanoparticles. *Water Conserv. Sci. Eng.* **2017**, *2*, 43–50. [[CrossRef](#)]
32. Bayomie, O.S.; Kandeel, H.; Shoeib, T.; Yang, H.; Youssef, N.; El-Sayed, M.M.H. Novel approach for effective removal of methylene blue dye from water using fava bean peel waste. *Sci. Rep.* **2020**, *10*, 7824. [[CrossRef](#)] [[PubMed](#)]
33. Patel, H.; Yadav, V.K.; Yadav, K.K.; Choudhary, N.; Kalasariya, H.; Alam, M.M.; Gacem, A.; Amanullah, M.; Ibrahim, H.A.; Park, J.-W.; et al. A Recent and Systemic Approach towards Microbial Biodegradation of Dyes from Textile Industries. *Water* **2022**, *14*, 3163. [[CrossRef](#)]
34. Gnanamoorthy, G.; Karthikeyan, V.; Ali, D.; Kumar, G.; Yadav, V.K.; Narayanan, V. Global popularization of CuNiO₂ and their rGO nanocomposite loveabled to the photocatalytic properties of methylene blue. *Environ. Res.* **2022**, *204*, 112338. [[CrossRef](#)] [[PubMed](#)]
35. Modi, S.; Yadav, V.K.; Gacem, A.; Ali, I.H.; Dave, D.; Khan, S.H.; Yadav, K.K.; Rather, S.-U.; Ahn, Y.; Son, C.T.; et al. Recent and Emerging Trends in Remediation of Methylene Blue Dye from Wastewater by Using Zinc Oxide Nanoparticles. *Water* **2022**, *14*, 1749. [[CrossRef](#)]
36. Choudhary, N.; Yadav, V.K.; Yadav, K.K.; Almohana, A.I.; Almojil, S.F.; Gnanamoorthy, G.; Kim, D.-H.; Islam, S.; Kumar, P.; Jeon, B.-H. Application of green synthesized mmt/ag nanocomposite for removal of methylene blue from aqueous solution. *Water* **2021**, *13*, 3206. [[CrossRef](#)]
37. Azzaz, A.; Jellali, S.; Hamed, N.; El Jery, A.; Khezami, L.; Assadi, A.; Amrane, A. Photocatalytic treatment of wastewater containing simultaneous organic and inorganic pollution: Competition and operating parameters effects. *Catalysts* **2021**, *11*, 855. [[CrossRef](#)]
38. Modi Shreya Fulekar, M.H. Green synthesis of zinc oxide nanoparticles using garlic skin extract and its characterization. *J. Nanostruct.* **2020**, *10*, 20–27. [[CrossRef](#)]
39. Jayarambabu, N. Germination and Growth Characteristics of Mungbean Seeds (*Vigna radiata* L.) affected by Synthesized Zinc Oxide Nanoparticles. *Int. J. Curr. Eng. Technol.* **2014**, *4*, 5.
40. Shamhari, N.M.; Wee, B.S.; Chin, S.F.; Kok, K.Y. Synthesis and characterization of zinc oxide nanoparticles with small particle size distribution. *Acta Chim. Slov.* **2018**, *65*, 578–585. [[CrossRef](#)]
41. Talam, S.; Karumuri, S.R.; Gunnam, N. Synthesis, Characterization, and Spectroscopic Properties of ZnO Nanoparticles. *ISRN Nanotechnol.* **2012**, *2012*, 372505. [[CrossRef](#)]

42. Khan, S.H.; Pathak, B.; Fulekar, M.H. Synthesis, characterization and photocatalytic degradation of chlorpyrifos by novel Fe: ZnO nanocomposite material. *Nanotechnol. Environ. Eng.* **2018**, *3*, 13. [\[CrossRef\]](#)
43. Khan, S.H.; Pathak, B.; Fulekar, M.H. A study on the influence of metal (Fe, Bi, and Ag) doping on structural, optical, and antimicrobial activity of ZnO nanostructures. *Adv. Compos. Hybrid Mater.* **2020**, *3*, 551–569. [\[CrossRef\]](#)
44. Khan, S.H.; Rajendran, S.; Pathak, B.; Fulekar, M.H. Development of zinc oxide nanoparticle by sonochemical method and study of their physical and optical properties. *AIP Conf. Proc.* **2016**, *1724*, 020108. [\[CrossRef\]](#)
45. Khan, S.H.; Yadav, V.K.; Ali, D.; Varghese, R. Influence of precursor ions on the structural morphological and optical properties of ZnO nanostructure and cytotoxicity on murine NIH 3T3 cells. *Chem. Pap.* **2022**, *76*, 477–489. [\[CrossRef\]](#)
46. Talodthaisong, C.; Plaeyao, K.; Mongseetong, C.; Boonta, W.; Srichaiyapol, O.; Patramanon, R.; Kayunkid, N.; Kulchat, S. The decoration of ZnO nanoparticles by gamma aminobutyric acid, curcumin derivative and silver nanoparticles: Synthesis, characterization and antibacterial evaluation. *Nanomaterials* **2021**, *11*, 442. [\[CrossRef\]](#) [\[PubMed\]](#)
47. Haque, J.; Bellah, M.; Hassan, R.; Rahman, S. Synthesis of ZnO nanoparticles by two different methods & comparison of their structural, antibacterial, photocatalytic and optical properties. *Nano Express* **2020**, *1*, 010007. [\[CrossRef\]](#)
48. Aldalbahi, A.; Alterary, S.; Almoghim, R.A.A.; Awad, M.; Aldosari, N.; Alghannam, S.F.; Alabdan, A.N.; Alharbi, S.; Alateeq, B.A.M.; Al Mohsen, A.A.; et al. Greener Synthesis of Zinc Oxide Nanoparticles: Characterization and Multifaceted Applications. *Molecules* **2020**, *25*, 4198. [\[CrossRef\]](#)
49. Sadak, M.S.; Bakry, B.A. Zinc-oxide and nano ZnO oxide effects on growth, some biochemical aspects, yield quantity, and quality of flax (*Linum uitatissimum* L.) in absence and presence of compost under sandy soil. *Bull. Natl. Res. Cent.* **2020**, *44*, 98. [\[CrossRef\]](#)
50. Siddiqi, K.S.; Rahman, A.U.; Tajuddin; Husen, A. Properties of Zinc Oxide Nanoparticles and Their Activity Against Microbes. *Nanoscale Res. Lett.* **2018**, *13*, 141. [\[CrossRef\]](#)
51. Rambabu, K.; Bharath, G.; Banat, F.; Show, P.L. Green synthesis of zinc oxide nanoparticles using Phoenix dactylifera waste as bioreductant for effective dye degradation and antibacterial performance in wastewater treatment. *J. Hazard Mater.* **2021**, *402*, 123560. [\[CrossRef\]](#) [\[PubMed\]](#)
52. Król, A.; Pomastowski, P.; Rafińska, K.; Railean-Plugaru, V.; Buszewski, B. Zinc oxide nanoparticles: Synthesis, antiseptic activity and toxicity mechanism. *Adv. Colloid Interface Sci.* **2017**, *249*, 37–52. [\[CrossRef\]](#)
53. Chiang, C.-T.; Roberts, J.T. Surface Functionalization of Zinc Oxide Nanoparticles: An Investigation in the Aerosol State. *Chem. Mater.* **2011**, *23*, 5237–5242. [\[CrossRef\]](#)
54. Ringu, T.; Ghosh, S.; Das, A.; Pramanik, N. Zinc oxide nanoparticles: An excellent biomaterial for bioengineering applications. *Emergent Mater.* **2022**, *5*, 1629–1648. [\[CrossRef\]](#)
55. Manojkumar, U.; Kaliannan, D.; Venkatesan, S.; Balasubramanian, B.; Kamyab, H.; Mussa, Z.H.; Jayanthi, P.; Mesbah, M.; Chelliapan, S.; Palaninaicker, S. Green synthesis of zinc oxide nanoparticles using *Brassica oleracea* var. botrytis leaf extract: Photocatalytic, antimicrobial and larvicidal activity. *Chemosphere* **2023**, *323*, 138263. [\[CrossRef\]](#)
56. Savassa, S.M.; Duran, N.M.; Rodrigues, E.S.; de Almeida, E.; van Gestel, C.A.M.; Bompadre, T.F.V.; de Carvalho, H.W.P. Effects of ZnO Nanoparticles on *Phaseolus vulgaris* Germination and Seedling Development Determined by X-ray Spectroscopy. *ACS Appl. Nano Mater.* **2018**, *1*, 6414–6426. [\[CrossRef\]](#)
57. Adrees, M.; Khan, Z.S.; Hafeez, M.; Rizwan, M.; Hussain, K.; Asrar, M.; Alyemeni, M.N.; Wijaya, L.; Ali, S. Foliar exposure of zinc oxide nanoparticles improved the growth of wheat (*Triticum aestivum* L.) and decreased cadmium concentration in grains under simultaneous Cd and water deficient stress. *Ecotoxicol. Environ. Saf.* **2021**, *208*, 111627. [\[CrossRef\]](#)
58. Tondey, M.; Kalia, A.; Singh, A.; Dheri, G.; Taggar, M.; Nepovimova, E.; Krejcar, O.; Kuca, K. Seed priming and coating by nano-scale zinc oxide particles improved vegetative growth, yield and quality of fodder maize (*Zea mays*). *Agronomy* **2021**, *11*, 729. [\[CrossRef\]](#)
59. Yadav, V.K.; Amari, A.; Wanale, S.G.; Osman, H.; Fulekar, M.H. Synthesis of Floral-Shaped Nanosilica from Coal Fly Ash and Its Application for the Remediation of Heavy Metals from Fly Ash Aqueous Solutions. *Sustainability* **2023**, *15*, 2612. [\[CrossRef\]](#)
60. Chaba, J.M.; Nomngongo, P.N. Effective adsorptive removal of amoxicillin from aqueous solutions and wastewater samples using zinc oxide coated carbon nanofiber composite. *Emerg. Contam.* **2019**, *5*, 143–149. [\[CrossRef\]](#)
61. Al-Musawi, T.J.; Yilmaz, M.; Ramírez-Coronel, A.A.; Al-Awsi, G.R.L.; Alwaily, E.R.; Asghari, A.; Balarak, D. Degradation of amoxicillin under a UV or visible light photocatalytic treatment process using Fe₂O₃/bentonite/TiO₂: Performance, kinetic, degradation pathway, energy consumption, and toxicology studies. *Optik* **2023**, *272*, 170230. [\[CrossRef\]](#)
62. Al-Musawi, T.J.; Alghamdi, M.I.; Alhachami, F.R.; Zaidan, H.; Mengelizadeh, N.; Asghar, A.; Balarak, D. The application of a new recyclable photocatalyst γ -Fe₂O₃@SiO₂@ZIF8-Ag in the photocatalytic degradation of amoxicillin in aqueous solutions. *Environ. Monit. Assess.* **2023**, *195*, 372. [\[CrossRef\]](#) [\[PubMed\]](#)
63. Fernández-Pérez, A.; Valdés-Solís, T.; Marbán, G. Visible light spectroscopic analysis of Methylene Blue in water; the resonance virtual equilibrium hypothesis. *Dye. Pigment.* **2019**, *161*, 448–456. [\[CrossRef\]](#)
64. Nguyen, N.T.; Nguyen, V.A. Synthesis, Characterization, and Photocatalytic Activity of ZnO Nanomaterials Prepared by a Green, Nonchemical Route. *J. Nanomater.* **2020**, *2020*, 1768371. [\[CrossRef\]](#)
65. Fouda, A.; Eid, A.M.; Abdelkareem, A.; Said, H.A.; El-Belely, E.F.; Alkhalifah, D.H.M.; Alshallash, K.S.; Hassan, S.E.-D. Phyco-Synthesized Zinc Oxide Nanoparticles Using Marine Macroalgae, *Ulva fasciata* Delile, Characterization, Antibacterial Activity, Photocatalysis, and Tanning Wastewater Treatment. *Catalysts* **2022**, *12*, 756. [\[CrossRef\]](#)

66. Fouda, A.; Salem, S.S.; Wassel, A.R.; Hamza, M.F.; Shaheen, T.I. Optimization of green biosynthesized visible light active CuO/ZnO nano-photocatalysts for the degradation of organic methylene blue dye. *Heliyon* **2020**, *6*, e04896. [[CrossRef](#)]
67. Kahsay, M.H.; Tadesse, A.; RamaDevi, D.; Belachew, N.; Basavaiah, K. Green synthesis of zinc oxide nanostructures and investigation of their photocatalytic and bactericidal applications. *RSC Adv.* **2019**, *9*, 36967–36981. [[CrossRef](#)]
68. Patwa, R.; Saha, N.; Saha, P. Green synthesis of zinc oxide nanoparticles, their characterization and utilization for photocatalytic removal of methylene blue. *Pray. Rasayan* **2021**, *5*. [[CrossRef](#)]
69. Lu, J.; Ali, H.; Hurh, J.; Han, Y.; Batjikh, I.; Rupa, E.J.; Anandapadmanaban, G.; Park, J.K.; Yang, D.-C. The assessment of photocatalytic activity of zinc oxide nanoparticles from the roots of *Codonopsis lanceolata* synthesized by one-pot green synthesis method. *Optik* **2019**, *184*, 82–89. [[CrossRef](#)]
70. Modi, S.; Fulekar, M.H. Synthesis and characterization of zinc oxide nanoparticles and zinc oxide/cellulose nanocrystals nanocomposite for photocatalytic degradation of Methylene blue dye under solar light irradiation. *Nanotechnol. Environ. Eng.* **2020**, *5*, 18. [[CrossRef](#)]
71. Elfeky, A.S.; Salem, S.S.; Elzaref, A.S.; Owda, M.E.; Eladawy, H.A.; Saeed, A.M.; Awad, M.A.; Abou-Zeid, R.E.; Fouda, A. Multifunctional cellulose nanocrystal/metal oxide hybrid, photo-degradation, antibacterial and larvicidal activities. *Carbohydr. Polym.* **2020**, *230*, 115711. [[CrossRef](#)] [[PubMed](#)]
72. Fagier, M.A. Plant-Mediated Biosynthesis and Photocatalysis Activities of Zinc Oxide Nanoparticles: A Prospect towards Dyes Mineralization. *J. Nanotechnol.* **2021**, *2021*, 6629180. [[CrossRef](#)]
73. Fouda, A.; Hassan, S.E.-D.; Saied, E.; Hamza, M.F. Photocatalytic degradation of real textile and tannery effluent using biosynthesized magnesium oxide nanoparticles (MgO-NPs), heavy metal adsorption, phytotoxicity, and antimicrobial activity. *J. Environ. Chem. Eng.* **2021**, *9*, 105346. [[CrossRef](#)]

Disclaimer/Publisher's Note: The statements, opinions and data contained in all publications are solely those of the individual author(s) and contributor(s) and not of MDPI and/or the editor(s). MDPI and/or the editor(s) disclaim responsibility for any injury to people or property resulting from any ideas, methods, instructions or products referred to in the content.